2009

The Production and Filtration Efficiency Testing of Nonwoven Electrospun Fiber Mats

Jan Uecker
Virginia Commonwealth University

THE PRODUCTION AND FILTRATION EFFICIENCY TESTING OF NONWOVEN ELECTROSPUN FIBER MATS

A thesis submitted in partial fulfillment of the requirements for degree of Master of Science at Virginia Commonwealth University.

By

JAN C. UECKER
Bachelors in Physics, Longwood University, 2007

Director: Gary C. Tepper
PROFESSOR, MECHANICAL ENGINEERING

Virginia Commonwealth University
Richmond, VA
July, 2009

Acknowledgement

The author would like to thank his advisor Dr. Gary Tepper for his guidance and motivation. I would also like to thank my research group, Dr. Dmitry Pestov, Azzad Elshazly and Ken Chien-Cheng for their assistance and advice. I would especially like to thank Dr. Joan Rosell for his guidance, support, and mentorship throughout this project. Finally, I wish to thank my parents, Dr. Arwed Uecker and Teresa Uecker, for their love and support as well as for encouraging me to pursue a graduate degree.

Table of Contents

List of Tables

List of Figures

Abstract

THE PRODUCTION AND FILTRATION EFFICIENCY TESTING OF NONWOVEN ELECTROSPUN FIBER MATS

By Jan C. Uecker, Master of Science

A thesis submitted in partial fulfillment of the requirements for degree of Master of Science at Virginia Commonwealth University.

Virginia Commonwealth University, 2009

Director: Dr. Gary Tepper, Professor, Department of Mechanical Engineering

In this thesis the production and filtration performance of electrospun nylon-4,6 nanofiber mats was experimentally studied. The average fiber diameter of nylon-4,6 fibers is controlled by altering the polymer concentration in solution. Adding small amount of pyridine to the electrospinning solution controlled fiber beading and other defects. These fibers were then deposited onto a wide variety of conductive and dielectric substrate materials. A corona ion source was used to eliminate surface charging effects observed at the surface of all substrates. The resulting fiber mats, uniform in size and distribution as verified by SEM imaging, are tested for filtration efficiency and pressure drop. A Figure of Merit (FOM) is calculated for each filter produced and compared to high-grade commercial filters.

CHAPTER 1
INTRODUCTION AND THEORY

1.1 Introduction

Nanotechnology is a rapidly expanding field of science having the objective of creating and controlling structures that are less then 100 nm in at least one dimension. One area of specific interest within the field is the controlled formation of one-dimensional (1D) nanostructures. These structures have the potential for unique characteristics not found in their micro or macro scale counterparts and therefore hold the promise of improving, perhaps reinventing, many commercial applications which have in the past reached scale limitations.

There are a large number of methods by which 1D nanostructures, including fibers, rods, and tubes in a variety of materials, can be generated.[1,2] These techniques include drawing[3], phase separation[4] , self-assembly[5], etc. The drawing process is a method by which a very long single fiber is produced, and is very similar to dry spinning as used in commercial fiber production. The major drawback of this method is that are a very limited number of raw materials that can be used. The material must exhibit very strong visco-elastic properties to ensure cohesion during the high stress induced during

elongation. The phase separation process involves dissolving a polymer and allowing the solution to form a gelatin. The bulk material is then extracted via another solvent, frozen and dried. The result is a foam-like substance with nano-scale pores. The process is very time consuming and only allows for the formation of very short nanofibers. The self-assembly process involves the predetermined assembly of nano-scale components into defined structures. Much like phase separation, the process is time consuming and does not allow for producing continuous fibers.

For many industrial applications the aforementioned methods for fiber fabrication are considered inefficient due to the high cost and long time required in producing even single fibers. Producing continuous fibers in bulk is nearly impossible using these methods. One particular technique that has shown great potential in overcoming these obstacles is electrospinning. Here electrostatic forces are used to initiate a polymer jet, which is elongated and solidifies before being collected. Although this method was first patented by Formhals over seventy years ago [6], there has been a renewed interest within the past two decades. The principle reason for this is that it allows for continuous fibers with diameters of less than 100nm to be produced [7]. Electrospinning is also considered to be a highly efficient method for producing fibers because the set-up and operational cost are relatively low while the output is very high.

The use of nano and micro fibers produced by the electrospinning method has been suggested as a viable candidate for a variety of applications in a number of fields. These include composites, protective clothing, wound dressing and tissue engineering, optics,

and high performance filtration. Filtration, in particular, is one field in which the use of electrospun fibers is especially promising, as it is necessary in a wide range of commercial applications and engineering fields. It has been estimated that the filtration market will be as high as US $700 billion by the year 2020[8]. The use of fibrous materials in filtration media has the potential to provide high filtration efficiency while minimizing pressure drop [9]. Filtration efficiency, as well as air resistance, has a strong correlation to the thickness of fiber employed. Commercial high efficiency filters are required to capture particles smaller than 0.3 micron in diameter. The pore size and the structural elements of a filter must be at the same size as the particles being captured in order to achieve high efficiency [10]. This combined with the fact that electrospun fiber mats have a very high surface to volume ratio make them ideal for capturing particles bellow 0.5 micron.

1.2 The Electrospinning Process

In electrospinning a high voltage is applied to a liquid drop that forms as a polymer solution is forced out of a flat-terminated hypodermic needle. At a given distance from the needle, a collection device is positioned which is either grounded or has a charge applied with opposite polarity to that of the needle. If the electrostatic field between the needle and the collector is at a sufficient potential to overcome the surface tension of the droplet a jet is formed. If the polymer solution used has low viscosity the jet will break up into small charged particles that are deposited on the collector. This is known as electrospray. If, on the other hand, the solution is relatively viscous the jet will not break

up and can be elongated into a very thin fiber. This fiber and the resulting collected mat will have varying size and uniformity based on process parameters which include the polymer concentration, applied voltage, needle to collector distance, and polymer flow rate.

In order to understand the fundamental principle of electrospinning it is beneficial to explore a simplified model based on a single droplet. Consider a single charged droplet composed of a conducting liquid polymer solution of low molecular weight. Further constraints include a perfectly spherical shape and that the droplet is held in vacuum. In this simplified case the droplet is influenced by two forces: the surface tension γ that confines the droplet to a spherical shape and the electrostatic repulsive force induced by the charging of the liquid. These two forces act in opposing directions with respect to the sphere. The surface tension produces a radially inward force while the electrostatic repulsive force acts radially outward. When these two forces are equal to one another, or at equilibrium, the resulting net force is given by:

$$\frac{1}{8\pi\varepsilon_o}\frac{Q^2}{R^2} = 8\pi\sigma_s R$$

where, Q is the electrostatic surface charge, R is the radius of the sphere, ε_o is the dielectric permeability of vacuum, and σ_s is the coefficient of surface tension.

As the strength of the electrostatic field surrounding the droplet is increased the amount of charge concentrated at the surface increases. The repulsive force induced by the increasing surface charge will eventually overcome the surface tension force as this force remains static. When this critical point is reached the net force is positive in the radially outward direction causing the droplet to break up into multiple smaller droplets. This is known as a Coulomb explosion. This process can repeat itself multiple times as the external electrostatic field continues to increase, creating smaller particles at each iteration. This is the principle mechanism by which electospray operates.

Considering another situation that is identical to the one outlined above with the exception of a high molecular weight polymer solution, the result is quite different. As the molecular weight of a polymer increases the molecular chain length also increases. This increases the probability that molecular chains will become entangled within solution. These molecular chain entanglements do not allow the droplet to disintegrate as they provide mechanical stability to the polymer solution. Instead of droplets a jet can be formed which over a sufficiently high distance will solidify into a filament, or fiber.

These fundamental principles of fiber formation can be expanded to state the working principles behind a conventional electrospinning setup. A high electric potential is applied to a droplet of polymer solution suspended from the end of a nozzle. This electric potential induces an electrostatic charge on the solution. If the field is sufficiently small the surface tension of the droplet is strong enough to maintain mechanical stability. At higher electric potential the surface charge on the droplet is also high. The resulting

increase in electrostatic repulsive charge is higher than the surface tension and the droplet is deformed into a conical shape commonly known as a Taylor cone.[11] As the strength of the electrostatic field surpasses a certain threshold value the electrostatic force will overcome the surface tension forcing a liquid jet from the nozzle. The jet then undergoes a whipping and stretching process leading to the formation of a thin fiber. This whipping and elongation process allows time for the solvent to evaporate and the fiber can decrease in size from several hundred micrometers to less than 10 nanometers.[12] The fibers are attracted by a grounded plate and are generally collected in randomly oriented, non-woven mats.

1.2.1 Early Work in Electrospinning

The study of the charged liquid droplet stability and the subsequent formation of electrostatically driven jets has been under investigation for many years. The first to document and describe the formation of jets driven by electrical forces was Bose in 1745.[13] His work was later expanded upon by Lord Rayleigh who in 1882 described the various process parameters by which jets within electric fields are influenced.[14] At the turn of the 20th century the first works emerged describing the relationship between the surface tension of a liquid and the surface charging by electric fields. In 1917, Zeleny described how the surface tension of a droplet could be overcome by surface charging leading to both jet formation and Coulomb expansion.[15] These works established the fundamental principles for both electrospay and electrospinning. After this point further

research became more specialized leading to the development of the two distinct, but closely related, techniques.

The process of electrospining, as it is known today, was first patented by Formhals in 1934.[6] At the time process was termed “electrostatic spinning”, it was not commonly referred to as “electrospinning” until the early 1990s. In his patent, Formhals describes a method by which thin threads could be formed from a polymer jet using electrostatic forces. Cellulose acetate and ethylene glycol were mixed to form the polymer solution used. This solution was then introduced into an electric field as shown in Figure 1.1. In his apparatus several nozzles in series were used to inject the polymer solution into an electric field. These nozzles were connected to a reservoir that provided a continuous feed of solution. The collection device was a flexible metallic grid, acting as a belt, wrapped around two spinning drums. The electric field was established by connecting the negative terminal (anode) of a high voltage power supply to the nozzles while the positive terminal (cathode) was connected to the moving collection plate. As the solution was forced out of the spinnerets, charged jets of solution were formed which evaporated as they were drawn towards the collector. The remaining solid material was collected in the form of short spun fibers. The potential between the cathode and anode were adjusted for various concentrations of polymer solutions to ensure jet formation. The collected fibers stuck to both the collector as well as one another due to incomplete solvent evaporation across the short spinning distance. The resulting fiber mats were collected using a stripping apparatus.

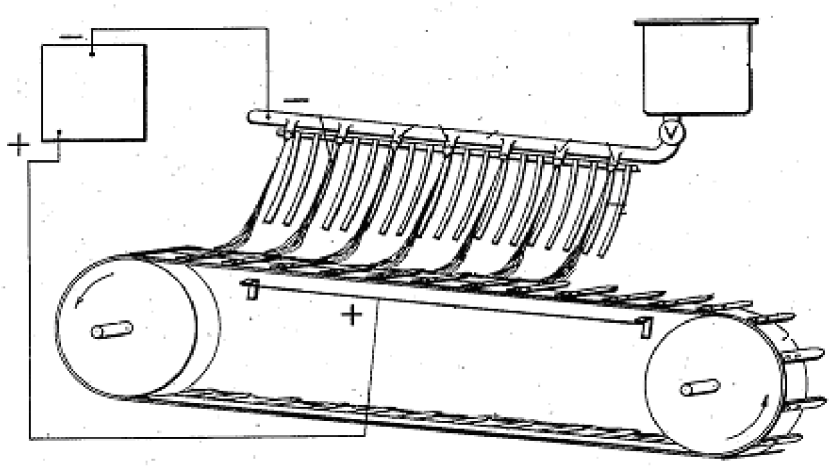

Figure 1.1 Schematic representation of Formhals' electrostatic spinning apparatus.[6]

Formhals' device proved to efficiently produce fibers but the difficulty in removing these fibers for further study or commercial applications was a major drawback. Because the fibers not only fused to one another but also to the collection device and wheels removing the fibers while keeping the mat intact was difficult and time consuming. In 1966, Simons provided a solution to this problem when he patented his own electrospinning apparatus.[15] The positive electrode was connected to the spinning solution while the negative electrode was placed on a collection belt. This belt was smooth and allowed for much easier removal of the fibers collected as a non-woven mat. Simons found that short, thin fibers could be collected using low viscosity polymer solutions while highly viscous solutions tended to produce continuous but relatively thick fibers.

In 1980, Guignard patented another electrospinning device based on two traveling belts opposite of one another, as in Figure 1.2. One belt was grounded and used as a collection device much like that of Simon. The other belt was used as the source of the polymer jets.

Instead of utilizing spinnerets, Guinards' device deposited the polymer solution directly onto a moving belt via a funnel. As the belt moved past the funnel a thin layer of solution was formed. High positive voltage was applied to this belt resulting in the formation of several jets at the polymer surface. These jets traveled a short distance to the other belt were the resulting fibers were collected. By placing a stripping plate at one end of the collection belt a continuous layer of non-woven electrospun fibers could be extracted. In l

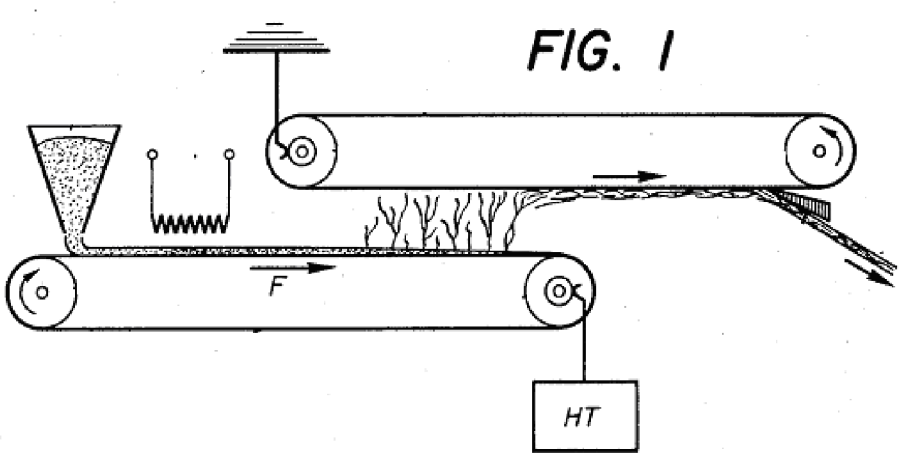

Figure 1.2 Schematic diagram of Guignard's electrospinning apparatus.[16,17]

During the same time, but in a different study, Dereck et al. began spraying both organic and polymer solutions using a single syringe. [18] These fibers were collected on both moving belts and stationary screens. Mats comprised of organic materials were suggested as possible wound dressings. In 1982, Bornat patented a method that expanded on the syringe method developed by Dereck. [19] As in Figure 1.3, several syringes in series were used to produce fibers that were then collected on a rotating drum. Each of the syringes

was filled with a polymer solution and was aligned at a certain distance from the collector. The collector consisted of a spinning metal rod driven by a belt and motor, to which a –50kV voltage was applied. Each of the syringes was grounded creating a electric potential. The fibers produced collected on the collector in the form of long continues fibers that wrapped around the drum. Solutions used included poly(tetraflouroethylene) and poly(ethylene oxide). In later work by Bornat et al. this concept was expanded in order to create composite materials used as filters.[20] Using a solution of polystyrene in methylene chloride fine fibers were electrospun onto movable belt. Much larger cellulose fibers where then deposited on top of these electrospun fibers using conventional spinning methods. The resulting composite fiber mats were suggested as being useful as high performance filters.

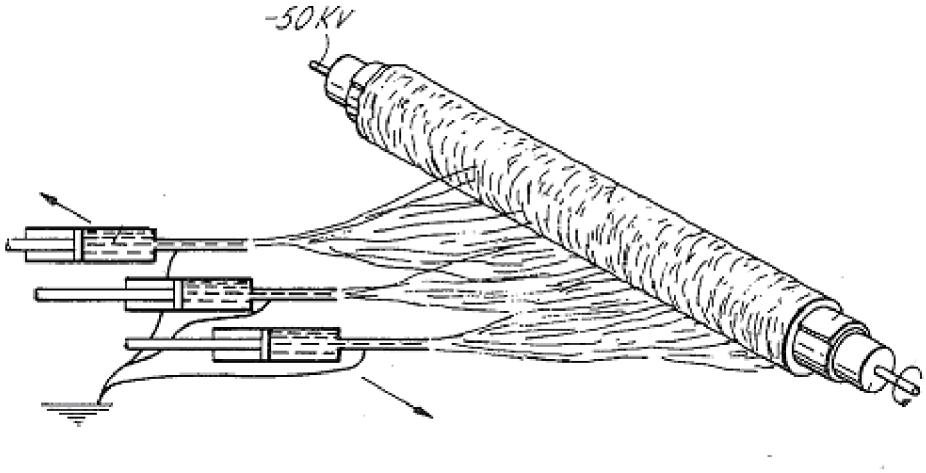

Figure 1.3 Schematic diagram of Bornat's electrospinning apparatus. [19]

There were very few advances in the field between the early 1980s until early 1990s when interest was renewed by Reneker and his fellow researchers. In 1995 Reneker

published work that described in detail the various process parameters critical to the formation of poly(ethylene oxide) fibers.[21] This prompted several other research groups to continue this work by similarly studying the process parameters of many of the other polymers that can be electrospun. To date hundreds of such polymers have been extensively studied. Much of this work will be discussed in the following sections.

1.2.2 Electrospinning Process Parameters

The electrospinning process, despite having several mechanical components, is fundamentally a fluid dynamics problem and can be studied as such. There are several process parameters that control the physical property, geometry and bulk production of electrospun fibers. It is important, therefore, to understand both physically and quantitatively how a polymer solution extruded through a capillary tube sever hundred micron in diameter is transformed into a nanofiber several orders of magnitude smaller. As a droplet is formed at the end of the capillary and the electrostatic field overcomes the surface tension a jet is formed which elongates until reaching the collector. This process can be divided into three stages [22]: jet initiation and extension, jet whipping and thinning, and jet solidification.

1.2.2.1 Jet Initiation and Extension

The basic principles of jet initiation where developed by Taylor in the early 1960s. Taylor showed that by applying an electrostatic force to conducting tubes containing

various liquids fine jets could be drawn.[23] Initially the fluid meniscus is nearly planer, however, as the electric potential of the capillary tube rises this layer becomes conical in shape and a fine jet is drawn.[24] Taylor described this formation of a jet as being attributed to the maximum instability of the liquid surface driven by the electric field. It was also shown that fluid will only be ejected if the cone has reached a minimum vertical angle of φ=49.3°. This specific type of cone is commonly known as a Taylor cone. The angle required for fluid ejection has been verified by Larrondo who experimentally showed a semi-vertical angle of just under 50°.[25]

Another important parameter to jet initiation is the magnitude of the electrostatic field required. Taylor also showed the critical voltage, V_c, at which maximum fluid instability of the droplet forming at the end of the electrospinning nozzle occurs. This is the minimum voltage at which a Taylor cone is formed. It is given by[24]

$$V_c^2 = 4\frac{H^2}{L^2}\left(\ln\frac{2L}{R} - 1.5\right)(0.117\pi R\gamma)$$

where H is the distance between the tube and collector , L is the length of the tube, R is the radius of the tube, and γ is the surface tension of the liquid. Hendricks at al. did a similar calculation based on a suspended droplet held in air given by[26]

$$V = 300\sqrt{20\pi r\gamma}$$

where r is the radius and γ is the surface tension of the liquid. If the substance surrounding material is some other nonconductive liquid the droplet distortion will be greater for a given electric field. The voltage required to initiate spinning in a vacuum, for example, will be lower.

1.2.2.2 Jet Whipping and Thinning

The process of jet whipping and thinning is not yet completely understood. Until as recently as 2001 it was generally believed that the principle reason for fiber thinning was due to branching of the jet as it is drawn towards the collector. Specifically it was believed that the main jet would split into sub-jets, a process that would repeat itself several times resulting in small fibers. This is known as “splaying”. Visual inspection of the “jet envelope” seemed to validate this, as it appeared fibers split in order to create a plum. (see Figure 1.4)

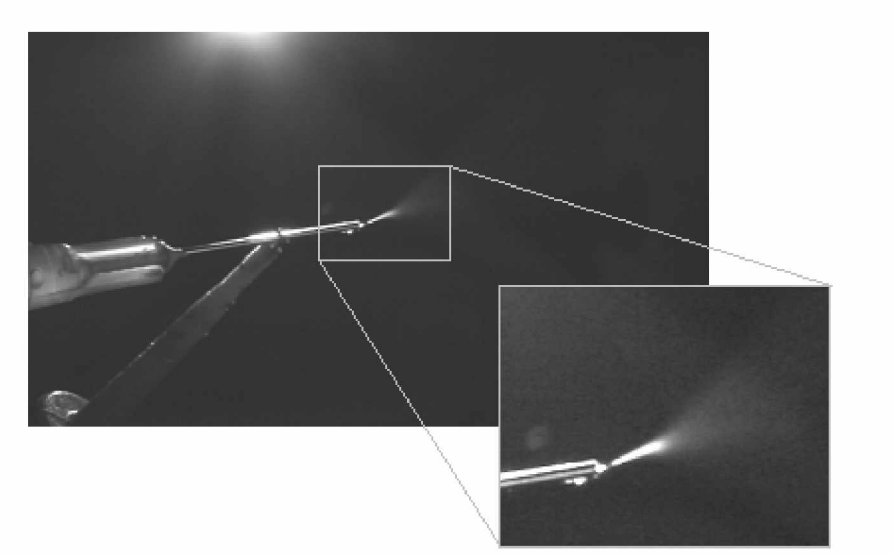

Figure 1.4 Optical photograph of jet plume during electrospinning.

While it is true that the electrospun jet can experience branching before being deposited on the collector, this is not the principle mechanism responsible for fiber thinning.

Recent studies involving high-speed cameras, have shown that fluid instability also occurs during this stage of electrospinning and that this is the primary driving force behind reducing the fiber diameter from the micrometer to nanometer scale. Here the jet undergoes a nonaxisymetric instability, or whipping, which causes the jet to be bent and stretch at high frequency.[27][28] As shown in Figure 1.5, this instability occurs after the formation of the Taylor cone and a short period of jet elongation.

Shin et al. investigated the jet instability of PEO (polyethylene oxide) and determined that there are three distinct types of instability that could exist; Reyleigh instability, axisymmetrical instability, and non-axisymmetrical instability. [29] The Rayleigh and

second axisymmetrical instability are very similar in nature in that the instability takes place uniformly with respect to the axis positioned at the tip of the Taylor cone. Non-axisymmetrical instability, also known as “whipping instability”, is driven primarily by the bending force. It was found that the electric field force determines the type and magnitude of instability. At low field strength Rayleigh instability was observed while at very high field strength whipping instability was noted.

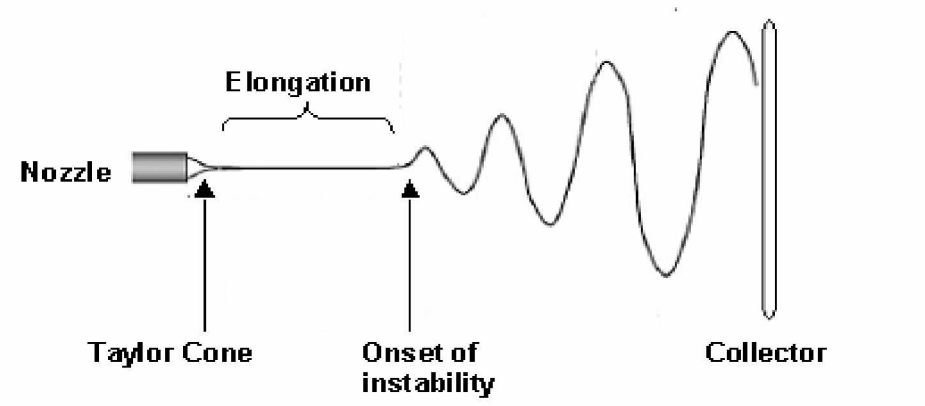

Figure 1.5 Schematic diagram of solution jet during electrospinning.

1.2.2.3 Jet Solidification

The process of jet solidification occurs as the electrospun fiber travels from the Taylor cone to the collector. During the elongation and instability of the polymer jet the solvent is evaporated. Since evaporation is, in part, a time dependant variable it is essential that the distance between the nozzle and collector is of sufficient length to allow for the fiber to completely dry. The magnitude of the electrostatic field is also critical as this drives jet instability. At higher field strength the jet will experience greater instability allowing more time for solvent evaporation. Other parameters that are critical in determining the

solidification rate include (a) solution properties such as conductivity, elasticity, viscosity and surface tension, (b) governing variables such as hydrostatic pressure in the nozzle and the electrostatic potential at the nozzle tip, and (c) ambient parameters including, environment and solution temperature, humidity, and air circulation.

Yarin et al. studied the jet solidification of several polymers and derived a one-dimensional equation describing the reduction in mass due to solidification and evaporation. It was calculated that a polymer solution with an initial weight concentration of 6% would produce a solid fiber with a cross-section $1.31x10^{-3}$ times that of the fluid jet.[30] It was determined that this solidification rate varied as the polymer concentration was altered.

1.3 Filtration Theory

In this section the various filtration capture modes and many of the most significant filter parameters will be discussed. The capture modes used in particle retention are described in order to give an understanding as to how particles are, in theory, captured by a single fiber of a filter. These concepts are then expanded upon to determine the most significant parameters of bulk filter media. The concepts can be directly related to filters comprised of electrospun fibers, as they behave in the same way as other fiber based filters produced using conventional methods. Finally, filtration standards will be reviewed in order to provide an understanding as to how filters are characterized and evaluated for commercial and other application.

1.3.1 Capture Modes

Various physical mechanisms are contributing factors in a high performance filter's ability to efficiently capture particles of various sizes. The most predominant capture modes include interception, inertial impaction and diffusion. Each of these mechanisms describes how a particle, following streamlines, is captured by one of the fibers comprising the filter. Contrary to common belief, however, a filter does not simply capture all particles above a given size. A filters ability to utilize a given mechanism is highly dependent on the particle size as well the air velocity under which the filter is operating.

Interception is a mechanism by which a particle, following gas streamlines, comes within one radii of a fiber. As the particle touches the fiber it adheres to it and is removed from the gas flow as shown in Figure 1.6a. Particles captured via this method typically have a radius above 0.4 μm. For any given particle size above this threshold certain streamlines will move close enough to a fiber to allow for capture. Streamlines that are further away than the radii of the particle will not contribute to this filtration mechanism.

Inertial impaction occurs when a particle is sufficiently large in size that it is unable to adjust quickly enough to the changing streamline directions near a fiber. This is due to the inertia associated with a moving particle of large size. Streamlines generally do not change direction until relatively close to the fiber. The particle will continue along its

original path and impact the fiber at high velocity as shown in Figure 1.6b. The particle will become imbedded in the fiber and thus be removed from the gas flow.

Diffusion is a mechanism that aids in the capture of small particles, <0.4 μm in size. In order to understand diffusion it is necessary to have an understanding of the kinetic theory of gasses. This theory describes that a gas is a collection of molecules that are very small in size relative to the distance between them. Ideally these particles behave like solid spheres that constantly move in straight lines. However, these particles do collide with one another randomly quite often resulting in a zigzag path. This motion is referred to as Brownian motion.[31] A particle being influence by diffusion behaves in much the same way. As the particle is carried by the gas flow it is constantly bumping into gas molecules and other particles resulting in a random motion through the filter media as shown in Figure 1.6c. Because the particle is moving in this motion instead of linearly along streamlines it spends more time inside the filter. This allows for a higher probability that the particle can be captured via one of the two capture methods, interception and impaction.[32]

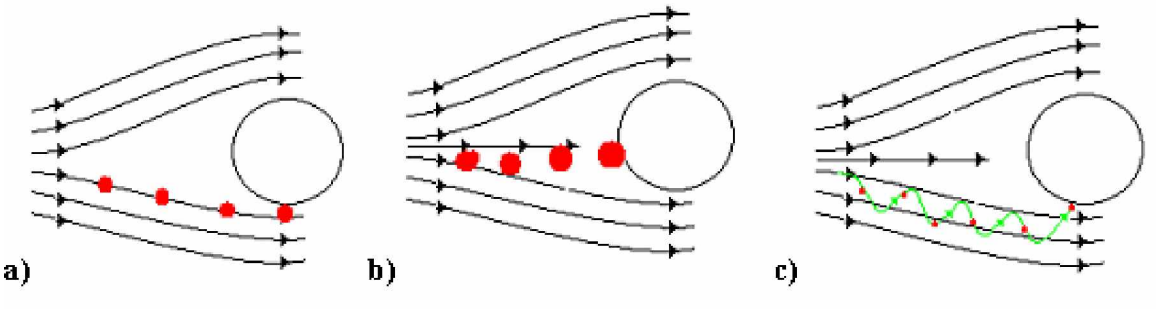

Figure 1.6 Schematic diagram of particle following stream lines towards a fiber. Three capture modes are presented; a) interception, b) inertial impaction and c) diffusion

These various filtration mechanisms are the reason a filters efficiency in removing particles from a gas stream is directly related to the size of the suspended particles. When the efficiency of capture is graphed against the particle size an upside down bell curve is generally observed. This is because particles of about 0.3 μm in size are very difficult to capture and will show an area of lower efficiency in the curve. Particles above this size can be captured by impaction and interception while smaller particles can be captured via the aid of diffusion. Particles 0.3 μm in size however are too small to be efficiently captured by interception and are too large, in comparison to air molecules, to allow for efficient diffusion.

1.3.2 Filter Parameters

The capture modes outlined in the previous section describe how a single fiber captures a particle. The concepts are now expanded upon to determine the parameters that play

significant rolls in the filtration efficiency of bulk fiber mats. These include: fiber size, mat thickness and solidity.

1.3.2.1 Fiber Size

Fiber size is an important parameter in evaluating filters as it is directly linked to the various capture modes under which filters operate. Smaller fibers are generally more efficient in capturing particles via interception while larger fibers aid in enhancing impaction capture. By changing the fiber size it is possible to fine tune which particle size the filter will be most efficient at capturing. It is however rare that all fibers in a filter have exactly the same size, i.e. monodispersed. Usually fibers will fall into a range of fiber sizes. This can occur for a variety of reasons. One example is when process parameters in the production of fibers are not kept sufficiently consistent leading to variations in size. Often, fibers of various sizes are also implemented out of mechanical necessity. Small fiber mats, which are generally thought to be highly efficient in capturing particles, do not have enough mechanical integrity to support themselves. Larger fibers may be added to provide this support.

Kirsch and Stenchkina using a complex variable approach applied to a filter of identical fibers solved the problem of mixing two particle sizes. They found that the pressure drop across such a filter could be approximated by the pressure drop of a single monodispereded layer of fibers having a diameter equal to the mean of the two fiber types. The flow pattern observed experimentally also very closely matched the

calculation.[33] These calculations are useful in modeling filters that have a relatively small spread in fiber diameters as is common in filters that have variances in size to fiber production inconsistencies. This is common in filters produced using the electrospinning method.

The fiber diameter is not only an important parameter in particle capture but is also very closely related to the pressure drop that a filter imparts on a gas flow. Filters made up of nanometer-scale fibers the pressure drop may be reduced greatly due to slip flow at the fiber surface [34]. Classical filtration theory assumes that there is continuous flow around a fiber with a "no-slip" condition at the surface. While this assumption is true for relatively large fibers, it does not hold for fiber diameters that begin to approach the scale of the molecular movements of air molecules. The Knudsen number can be used to describe the significance of molecular movement of air molecules at the surface of the fiber in relation to the overall flow field. The Knudsen number, K_n is given by:

$$K_n = \lambda / r_f$$

where λ gas mean free path, and r_f is the radius of the fiber. As K_n increases beyond a point at which it can be considered negligible the continuous flow theory becomes increasingly less valid. While there is not a precise cutoff point at which slip flow prevails it is generally considered at $Kn > 0.1$. The mean free path of air is approximately 0.066 μm meaning slip flow needs be considered for fiber diameters of < 0.5 μm. In a slip flow condition the air velocity at the fiber surface is considered to be non-zero. This translates into a lower pressure drop because drag is reduced in comparison to a no-slip

condition. This indicates that as the fiber size of a filter decreases bellow 0.5 µm the filtration efficiency improves for the same pressure drop.

1.3.2.2 Mat Thickness

Matt thickness in filtration referees to the total thickness of all layers of fibers that make up the filtration media. This does not necessarily include any substrates or other support media that does not aid in the retention of particles. Earlier the collection of particles by a single fiber was investigated. It makes sense, intuitively, to assume that a thicker layer of fibers will result in higher efficiency of the filter. This is true to a point. A thicker fiber matt will aid in the retention of particles, however, once a certain threshold is reached adding further fibers to the matt may not increase efficiency. The top layer of the filter may capture much of the particle concentration while the additional fibers serve no purpose in terms of further particle capture. In fact, as the matt thickness is increased the pressure drop across the filter also increases. Because filter performance is generally measured in filtration efficiency as a function of pressure drop, this added thickness will produce a poor overall performance. It is important therefore to make the filter as thin as possible, by not adding additional unneeded fiber layers.

1.3.2.3 Solidity

The solidity of a filter is defined as the ratio of solid material volume to the total filter volume. This can be expressed in the following equation:

$$\alpha = \frac{m_{filter} / \rho_{fiber}}{V_{filter}}$$

where α is the solidity, m is the filter mass, ρ is the fiber density, and V is the filter volume. Typical values range from 0.001 to 0.2. The solidity of the fiber matt is an important parameter as it is closely related to the slipstreams that surround individual fibers throughout the filter. The Kuwabara number gives the flow around a fiber, which is only dependent on solidity, and is expressed as

$$Ku = -\frac{\ln\alpha}{2} - \frac{3}{4} + \alpha - \frac{\alpha^2}{4}$$

This number is used in many equations that model impaction and interception of particles in a filter.[35] Because the slip streams around individual fibers determine the effectiveness of all three capture modes as well as the overall air permeability of the filter media, the solidity is an important parameter when evaluation filtration performance.

1.3.3 Review of Filtration Standards

Filtration standards are a critical component when evaluating a filter and comparing it to other commercially available filters. While a wide variety of testing standards exist this section will focus on the ones most commonly used in evaluating commercial filters used for air purification. Clean-room standards may be more stringent.

Three standards that are widely used internationally to evaluate commercially available filters include EN779:2002, ASHRAE 52.1, and ASHRAE 52.2. Both ASHRAE 52.2 and EN779:2002 incorporate tests for efficiency based on particle diameter. ASHRAE 52.1 includes tests for measuring the efficiency on the relatively coarse loading dust. EN779:2002 also provides testing of the filtration based on electrostatic charging of fibers. All these methods of testing result in a specific rating that can universally be used to compare various filters. They include High Efficiency Particulate Air filter, or HEPA, and Ultra Low Penetration Air filters, or ULPA.

HEPA was first developed as a standard during World War II. It was necessary at the time to develop high efficiency filters that could capture radioactive particles as well as chemical and biological warfare agents. This standard later grew to incorporate ratings for filters used in hospitals, electronics manufacturing, pharmaceuticals production and space exploration. Testing of these types of filters generally relies on the use of monodispersed particles having a diameter of 0.3 μm. This particle size is widely thought to be the most difficult to capture. It is the most penetrating particle diameter (MPPD). ULPA was developed more recently as newer filter media types have been invented. This rating system is more sensitive and incorporates testing over a wider range of particle sizes.[36]

Commonly the HEPA and ULPA ratings are given to filters that have a 99.97% and 99.999% efficiency, respectively, in capturing particles 0.3 μm in diameter. Actual

ratings can be much more specific. Table 1.1 outlines the various ratings, which range from HEPA 10-14 and ULPA 15-17.

HEPA- and ULPA-type Filters		
Filter Class	**Overall value for Entire Filter**	
	Efficiency, %	Penetration, %
H 10	85	15
H 11	95	5
H 12	99.5	0.5
H 13	99.95	0.05
H 14	99.995	0.005
U 15	99.9995	0.0005
U 16	99.99995	0.00005
U 17	99.999995	0.000005

Table 1.1 An outline of the HEPA and ULPA rating system. Particle size is 0.3 μm.

1.4 Concluding Remarks

In the preceding sections a brief introduction to the fundamental principles of electrospinning were provided. In addition, a literature review of the early works in electrospinning and electrospray was presented. Next, the underling principles of filtration theory as well as important parameters and standards were discussed. The ability to produce highly uniform fibers via the electrospinning method has generated

much interest over the past several years in the scientific community. Specifically, these types of fibers have shown great potential in their use as high efficiency filter mats. The following chapters (2-4) will present the research efforts of the author in which electrospinning has been utilized in the formation of fine fiber mats with high regularity and uniformity. It is also shown that fibers with diameters of bellow 100 nm can be produced. Filters produced from fibers at this scale benefit from the air slip flow condition at the fiber surface indicating that increased performance, over comparable filters with larger fiber diameters, may be seen.

Bibliography

1) Loscarteles A., Barrero A., Micro/Nano Encapsulation via Electrified Coaxial Liquid Jets Science 2002, 295, 1695.

2) Xia Y, Yang P. Guest editorial: Chemistry and physics of nanowire. Adv. Mater. 2003; 15: 351-456

3) Ondarcuhu T, Joachim C. Drawing a single nanofiber of hundreds of microns. Europhys Lett 1998;42(2):215-50

4) Ma P.X., Zhang R. Synthetic nano-scale fibrous extracellular matrix. J Biomed mat res 1999; 46:60-72.

5) Whitesides GM, Grzybowski B. Self-Assembly at all scales. Science 2002;295:2418-21.

6) Formhals, A.US, 2,123,992, 1934.

7) Huang C, Chen S, et. Al., Electrospun polymer nanofibres with small diameters. Nanotechnology 2006;17:1558-63

8) Suthat A, Chase G. Chemical Engineering, 2001, 26-8.

9) Tsaia PP, Schreuder-Gibson H, Gibson P. Journal of Electrostatics, 2002, 54 333-41.

10) Graham K, Ouyong M, Raether T, Grafe T, McDonald B, Knauf P. Fifteenth Annual Conference & Expo of the American Filtration & Separations Society, Galveston, TX; 9-12 April 2002.

11) Reneker D. H., Yarin A. L., Fong H., Applied Physics Letter, 2000, 87, 4531

12) Li D., Xia Y. Electrospinning of nanofibers: Reinventing the Wheel? Advanced Materials 2004; 16: 1151-70

13) Bose, G. M. Recheres sur la cause et sur la varitable theorie del'electricite: Wittenberg, 1745

14) Raleigh, L. London, Edinburgh, and Dublin Phil. Mag. J. 1882, 44, 184-186.

15) Simons, H. L. US, 3,280,229, 1996.

16) Guignard, C. US 4,230,650, 1980

17) Guignard, C. US, 4,287,139, 1981

18) Martin, G.H.; Dereck, I. US, 4,044,404, 1997

19) Bornat, A US, 4,323,525, 1982

20) Simm, W.L.; Claus, G. O.; Bonart, R. B.; Belta, V.F.G US, 4,069,026, 1978

21) Doshi, J.; reneker, D.H. Journal of Electrostatics 1995, 35, 151-160.

22) Dzenis YA, Wen YK. Continuous carbon nanofibers for nanofiber composites. Materials Research Society Symposium. Proceedings 2002; 702:173-8.

23) Taylor G.I. Disintegration of water drops in an electric field. Proc R Soc London, Ser A 1966;291:159.

24) Taylor G.I. Electricaly driven jets. Proc R Soc London, Ser A 1969; 313:453-75.

25) Larrondo, Manley r., St J. Electrostatic fiber spinning from polymer melts, I. The experimental observations on fiber formation and properties. J Polymer Science: Polymer Physics Edition 1981;19;909-20.

26) Hendricks Jr CD, Carson RS, Hogan JJ, Schneider JM. Photomicrography of electrically sprayed heavy particles. AIAA J 1964; 2(4):733-7.

27) Hohman MM, Shin M, Rutledge G, Brenner MP. Electrospinning and electrostaticaly forced jets. I. Stability Theory. Physics of Fluids 2001;13:2201-20.

28) Hohman MM, Shin M, Rutledge G, Brenner MP. Electrospinning and electrostaticaly forced jets. II. Applications. Physics of Fluids 2001;13:2221-36.

29) Shin YM, Hohman MM, Brenner MP, Rutledge GC. Electrospinning: A whipping fluid jet generates submicron polymer fibers. Appl Phys Lett 2001; 78:1149-51.

30) Yarin AL, Koombhongse S, Reneker DH. Bending instability in electrospinning of nanofibers. J Appl Phys 2001;89(5):3018-26.

31) Brown, Robert, "A brief account of microscopical observations made in the months of June, July and August, 1827, on the particles contained in the pollen of plants; and on the general existence of active molecules in organic and inorganic bodies." Phil. Mag. 4, 161-173, 1828.

32) Friedlander, S. K.. Smoke, Dust and Haze. 1st. New York: Wiley-Interscience, 1977. Print.

33) Kirsch, Stenchkina. A contribution to the theory of fibrous aerosol filters. Faraday Symposium of the Chemical Society, 7, 143, 1973.

34) Brown, R.C., Air Filtration, Pergamon Press, Oxford, 1993.

35) Lee, K.W and r. Mukund, 'Filter Collection". Aerosol Measurements, 2nd ed., P.A. Baron and k. Willeke, eds., Wiley, New york, 2001.

36) Tronville P.,"International Standards: filters for buildings and gas turbines" Filtration & Separation. Sept. 2005.

CHAPTER 2

EXPERIMENTAL APPARATUS

2.1 Introduction

Electrospinning of Nylon-4,6 was utilized in the production of micro and nano scale filtration mats. Fibers were spun at a variety of different polymer concentrations in solvent as well as onto a number of different substrates. These samples were then analyzed using a combination of optical and electron microscopy techniques in order to evaluate their morphologies. A corona enhancement method was developed to enhance the ability to spin onto certain substrates. Finally samples were tested for their filtration properties, including pressure drop, collection efficiency and figure of merit (FOM).

This chapter will outline the various materials used as well as provide descriptions and schematics of the production and analysis devices utilized in this study. This includes a description of polymer solutions and substrates, the electrospinning setup, the corona device, the filter test rig, and the imaging and analysis techniques. Certain operational conditions of the electrospinning setup will be outlined in greater detail in Chapter 3, which deals specifically with fiber morphology, mat morphology and the use of the corona.

2.2 Materials

2.2.1 Electrospinning Solutions

The electrospinning solution used in this study was nylon-4,6 (M_{repeat} 234.29 g/mol, T_M = 295 °C, ρ = 1.18 g/mL, Sigma-Aldrich 442992; CAS=50327-22-5) at various concentrations (8 Wt.% to 18 Wt.%) in formic acid (98%, Fluka 06440) to which 0.4 wt.% of pyridine (99%, Sigma-Aldrich 360570) was added. Materials are summarized in Table 2.1. All materials were used as received. The nylon, formic acid, and pyridine were combined in 10 or 40 mL vials and agitated using a sonicator (Branson, Model 2510) for a period of 4-6 hours at 40 °C to allow the solution to fully mix. It was observed that the solution darkened over time, however, no adverse effects were observed during electro spinning. Solutions were stored in a refrigerator for a period of up to one week before being discarded.

Polymer/Solvent	Molecular Formula	Molecular Weight, M_w	Density, g/cm^3	Source
Nylon-4,6	$(C_{10}H_{22}N_2O_4)_n$	10,000	1.18	Sigma-Aldrich
Pyridine	C_5H_5N	79.1	1.22	Sigma-Aldrich
Formic Acid, FA	CH_2O_2	46.02	0.978	Fluka

Table 2.1 Information about polymers & other chemicals used

Solutions were mixed at a variety of polymer concentrations. Certain electrospinning conditions were altered for each solution used. Table 2.2 summarizes these conditions. The voltage applied to the electro spinning needle was varied slightly and the flow rate was increased as the Wt.% of the polymer solution decreased. The needle to collector distance was fixed at 10 cm.

Polymers	Solvents	Pyridine Conc., wt %	Polymer Conc., wt %	Voltage, V_n	Flow rate, µl/mn	Needle to Collector Distance, cm
Nylon-4,6	FA	0.4	18	7.5	0.4	10
Nylon-4,6	FA	0.4	16	7.5	0.4	10
Nylon-4,6	FA	0.4	14	7.5	0.5	10
Nylon-4,6	FA	0.4	12	7.0	0.6	10
Nylon-4,6	FA	0.4	10	7.0	0.8	10
Nylon-4,6	FA	0.4	8	7.0	1.2	10

Table 2.2 Typical electrospinning conditions used in this study

2.2.2 Substrates

The electrospun fibers were deposited onto various substrate materials including cellulose filter paper (Whatman, CAT# 1093 126), polypropylene filter media (McMaster, FMS-1224-100), fiberglass mesh (New York Wire, Part #30117), polyester spunbound filter media (Reemay, Style No. 2014), ½" stainless steel mesh (Purpolator EFP, Part No. N87069A), nylon mesh (McMaster, 9318Txx), and polyester mesh (McMaster, 9218Txx). Substrates were cut into ½" discs or used as received. Table 2.3 summarizes

all materials used. Thread diameter, thread cross section, % open area, thickness, and opening width are reported. Measurements are reported from the manufacturers specifications or as directly measured using SEM images and/or a micrometer. All substrates are given a code which will be used when referring to any substrate in upcoming chapters.

Code	Material	Cloth type	Thread diameter (μm) [(1)]	Thread cross section	% Open Area [(2)]	Thickness (μm) [(3)]	Opening width (μm)	Part Number
P-20	Polyester	non-woven	20	trilobal	N/A	240	N/A	2014
PP-310	Polypropylene	woven	310	circular	N/A	565	N/A	FMS-1224-100
F-220	fiberglass	woven	220	circular	46	390	820	30117
C-30	Cellulose	non-woven	30-60	various	N/A	90	N/A	1093-126
N-50	Nylon	square weave	50	circular	36	82	75	9318T22
N-75	Nylon	square weave	75	circular	33	125	100	9318T21
N-120	Nylon	square weave	120	circular	53	200	325	9318T45
N-165	Nylon	square weave	165	circular	37	245	260	9318T16
N-305	Nylon	square weave	305	circular	37	480	480	9318T44
N-495	Nylon	square weave	495	circular	44	845	985	9318T28
P-225	Polyester	square weave	225	circular	49	350	535	9218T68
P-415	Polyester	square weave	415	circular	45	720	835	9218T13
SS-360	Stainless steel	square weave	360	circular	49	720	850	KC-28865090

Table 2.3 Substrate selections used. Notes: [(1)]For polyester non-woven, the diameter is based on the denier per filament provided by the manufacturer (DPF= 4.0). For the rest, thread diameter is based on measurements taken on SEM micrographs. [(2)]For square weave, %OA's are obtained from measurements taken on SEM micrographs.

[3]Manufacturer's spec for "polyester non woven"; other thicknesses are determined using a caliper.

2.3 Instruments

2.3.1 Electrospinning Apparatus

The electrospinning apparatus as described previously [1,2] was used with some modifications to the electrical wiring and collector. The setup is schematically outlined in Figure 2.1. The deposition of electrospun fibers was carried out on various types of substrates mounted using two small pieces of copper tape (typically 2 x 8 mm) onto an aluminum cylinder ("collector") prior to electrospinning. This cylinder measures 6.5 inches long, with 1" between parallel faces with each face having a width of 9/16". This cylinder was mounted to a lathe (Micro lathe II, Model 4500), and rotated at 1200 rpm (+/- 5%) via belt connection to an AC motor (Marathon Electric, Cat No. S102). Positioned at either side of the collector axis were an electrospinning needle and a corona assembly (Figure 2.2). The electrospinning needle consists of a stainless steel (SS) 23G needle (Becton-Dickinson, PrecisionGlide^{TM}) terminated flat to a length of approximately ½". It was connected to a 1 cc plastic syringe (National Scientific Company, #S7510-1) containing the polymer melt solution, and to a infusion pump (Harvard Apparatus PHD2000) run at various flow rates (0.4-1.2 µl/min). The tip of the needle was positioned 10 cm away from the axis of the collector. The needle, syringe and polymer solution were discarded after each days experiments. The corona assembly, was placed opposite side of

the collector. The assembly consists of a Teflon rod (19 mm dia., 55 mm length), a corona needle (Becton-Dickinson, PrecisionGlide^{TM}, 21G), and a corona shield (electroformed nickel mesh, 19 mm dia. wire welded in a square pattern with 4.5 mm^2 openings). The corona needle was connected to the center of one end of the Teflon rod and was soldered, internally, to a high voltage wire exiting through the opposite side. The wire shield was wrapped around the end of the rod, to cover the needle. The needle and wire mesh protrude 9 and 18 mm respectively from the rod. A positive potential, typically 7.5 kV, was applied to the electrospinning needle by a Matsusada Precision Inc. power supply (Model AMT-10810-LCS). A negative potential of typically –5.0 kV was applied to the corona assembly via a Spellman power supply (model CZE1000R). The collector and corona shielding were both electrically grounded. All voltage and current measurements were taken either directly from the power supplies or using an Agilent 34401A digital multimeter and/or a Fluke 80k-40 HV probe. Temperature and humidity measurements, taken before each experiment, were taken using a Vaisala HM 34 meter.

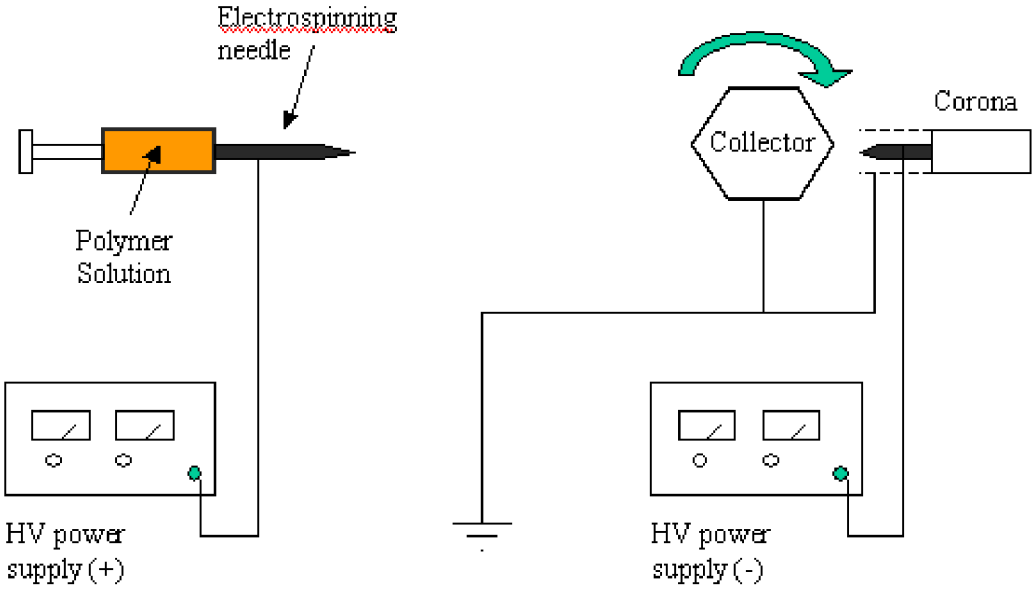

Figure 2.1 Schematic diagram of the electrospinning setup used

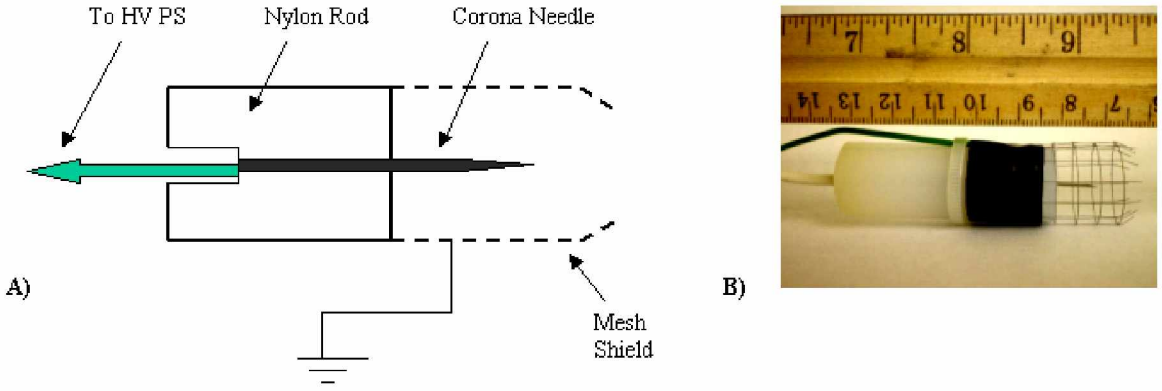

Figure 2.2 a) Schematic diagram and b) picture of corona assembly

2.3.2 Filter Test Rig

Fabricated filters, consisting of a substrate material cut to a ½" disc diameter and a layer of electrospun fibers, were tested using a testing apparatus consisting of the following: a filter test rig (FTR), two pressure transducers (Omega, models PX277-05D5V, PX277-0.1D5V), a rotameter (Cole-Parmer, model PMR1-010477), and optical particle counter (OPC, AeroTrak^{TM} model 8220).

The filter test rig, shown in Figure 2.3, consists of three pieces: upper, lower and inlet. The upper piece allows air to enter the FTR through a 1 cm long conical opening, having top and bottom diameters of 22.0 and 9.4 mm respectively and 30° edge. The rest of the piece has a center tapped bore which is 9.4 mm wide and 40 mm long. A pressure tap (wire gage size 76) between the inside bore and cylindrical outer surface is placed 38 mm from the top. The lower piece also has a 9.4 mm center tapped bore running the entire length. A bore of the same size is placed 80 mm from the bottom. The lower piece consists of a cylinder 12.6 mm in diameter and 50 mm in length with a center tapped conical opening on one end (32 mm in length, 11 mm top opening and 3 mm bottom opening. All pieces are constructed of stainless steel and fit together as shown in the figure. The inlet and lower piece are fitted together using a plastic ring. The filter is placed between the upper and lower piece with two o-rings placed on either side to ensure all air is forced through it.

As shown in figure 2.4 the pressure taps, located above and bellow the filter, are connected to the pressure transducers via Tygon® tubing (1/8" ID, ½" OD). This allows for upstream and downstream pressure measurements. The inlet piece allows airflow into the OPC and is connected with rubber tubing (supplied with OPC, 9 mm OD, 6 mm ID).

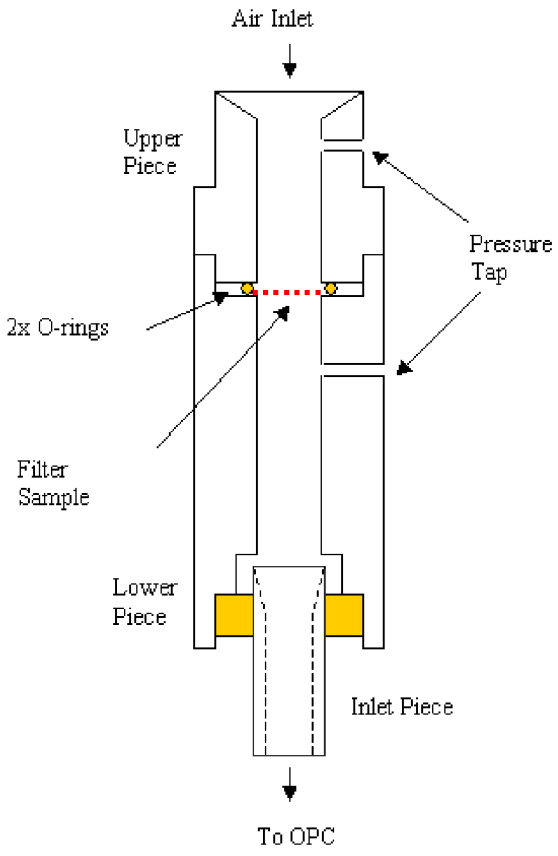

Figure 2.3 Schematic diagram of the Filter Test Rig.

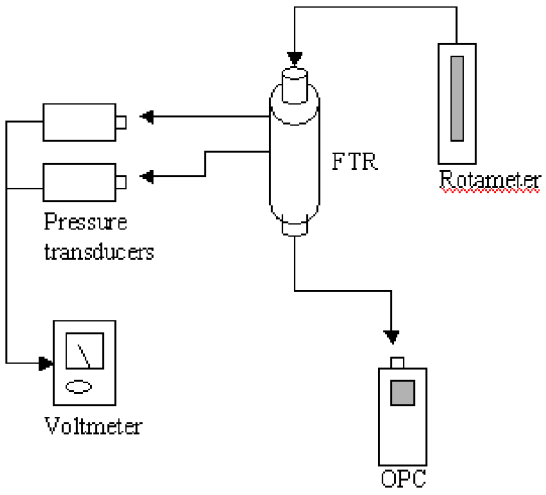

Figure 2.4 Flow diagram of filter testing setup.

2.3.3 Optical Particle Counter (OPC)

A AeroTrak^{TM} Handheld Optical Particle Counter (OPC), Model 8220 was used for all filtration efficiency measurements. A zero check was performed prior to every experiment using the supplied zero filter. The flow rate used was 2.8 lpm and was verified using the rotameter. The OPC has a particle size range of 0.3 to 10 μm and six user definable bin sizes with 0.01 μm increments. Counting efficiency is 50% ± 10% at 0.3μm and 100% ± 10% at 0.45 μm and greater. Unless otherwise noted measurements were taken with 0.3, 0.4, 0.7, 1.0 and 2.0 μm bin cutoffs (differential) and at 2 minute durations.

2.3.4 Scanning Electron Microscopy (SEM)

A Zeiss EVO 50 Scanning Electron Microscope was used in all electron based imaging. Unless otherwise noted the beam voltage was 30 kV, the probe current, I_{probe}, was 10 pA, the working distance, WD, was 3-10 mm, the detector bias was +400 V and the column aperture was 30 μm. All samples were mounted to aluminum sample holders using carbon adhesive tape. Samples were sputter coated in gold using an Electron Microscopy Sciences Model EMS550X Au sputter coater at $9x10^{-2}$ mbar and 30 uA.

2.3.5 Optical Microscopy

A OPELCO model Olympus BX60 microscope was used for all optical imaging. Images were taken at 5X, 10X, 20X and 50X magnification with top lighting. A Infinity 1-3C CCD camera was used to capture all images.

2.4 Data Analysis Methods

Pressure drop, Δp, was calculated by taking the difference between upstream and downstream pressure readings. Voltage output from the pressure transducers were displayed using multimeters (Meterman 5XL) and converted to units of Pascals unless otherwise noted. The filtration efficiency, P, was obtained by taking the difference between background particle counts (no filter) and filtered particle counts. Filtration efficiency is equal to 1- penetration, where the penetration P is defined as

$$P = \frac{\text{particle concentration upstream of the filter}}{\text{particle concentration downstream of the filter}}$$

Both counts were taken using the same flow rates and OPC settings. The figure of merit, Q, for all filters tested was calculate using the following formula:

$$Q = \frac{-\ln(P)}{\Delta p}$$

All pressure drop readings, filtration efficiencies, and figure of merits were plotted using Microsoft Excel. All optical and SEM images were analyzed using ImageJ version 1.40 (by Wayne Rasband, National Institute of Health) and Zeiss SmartSEM™ respectively. All OPC readings were recorded using TSI TrakPro™ Data Analysis Software.

Bibliography

1) Sarkar S., S. Deevi, G. Tepper, “Biased AC Electrospinning of Aligned polymer nanofibers”, Macromol. Rapid Commun, 28, 1034-9, 2007.

2) Kessick R., J. Fenn, G. Tepper, “The use of AC potentials in electrospraying and electrospinning processes”, Polymer, 45, 2981-84, 2004.

CHAPTER 3

ELECTROSPUN FIBER DEPOSITION

3.1 Introduction

Fibers of nylon-4,6 were electrospun at polymer weight concentrations ranging from 8% to 18% in solution. The variations in polymer concentration allowed for the formation of fibers with specific diameters. Then fibers were then deposited onto a polyester substrate and the physical characteristics of the resulting fibers were investigated. Individual fibers initially exhibited certain unwanted characteristics, such as the formation of beads Pyridine was added to the electrospinning polymer solution to eliminate these effects. The resulting fibers, uniform in size and free of any visible defects, were deposited onto a variety of substrates at different deposition times. The morphology of the resulting fiber mat was investigated and several observations were made. Under certain conditions physical interlinking between fibers occurred, fibers were not deposited uniformly on most substrate, and fibers appeared to be repelled by dielectric substrates with relatively small areas. These effects were determined to be caused by surface charging of the substrates. A corona ion source was then added to the electrospinning apparatus to electrically neutralize the substrates. Using this modified setup, fiber repulsion by substrates was reduced and fiber mats exhibit enhanced uniformity.

3.2 Fiber morphology

3.2.1 Controlling fiber size

The smallest conventional nylon fibers produced by conventional spinning have a linear density of around 1.7 dtex, corresponding to a fiber diameter of about 30 μm.[1] The diameter of electrospun Nylon-4,6 fibers used in this work range from about 300 nm to 75 nm. The diameter was controlled by adjusting the nylon concentration of the electrospinning solution. Table 3.1 lists all of the polymer concentrations used in this work.

Nylon-4,6 concentration (wt. %)	8	10	12	14	16	18
Diameter of fiber (nm)	75 ± 5	99 ± 6	126 ± 7	147 ± 12	206 ± 21	265 ± 21

Table 3.1 The average diameter of fibers, in nm, as a function of weight % concentration of Nylon,4-6 in solvent.

The electrospun fibers were produced from a jet of polymer solution as described in Chapter 2, Section 3.9.1. Solutions of low nylon concentrations elongated more before drying due to the low nylon to solvent ratio resulting in thin fibers. In contrast, fibers produced by solutions of high nylon concentration had a shorter period of elongation, due

to less formic acid being evaporated before solidifying, and were thus thicker. Electron microscopy images of fibers produced from all nylon concentrations were obtained, and thick fibers were observed at high concentration and thin fibers are observed at low concentration, shown in Figure 2.1.

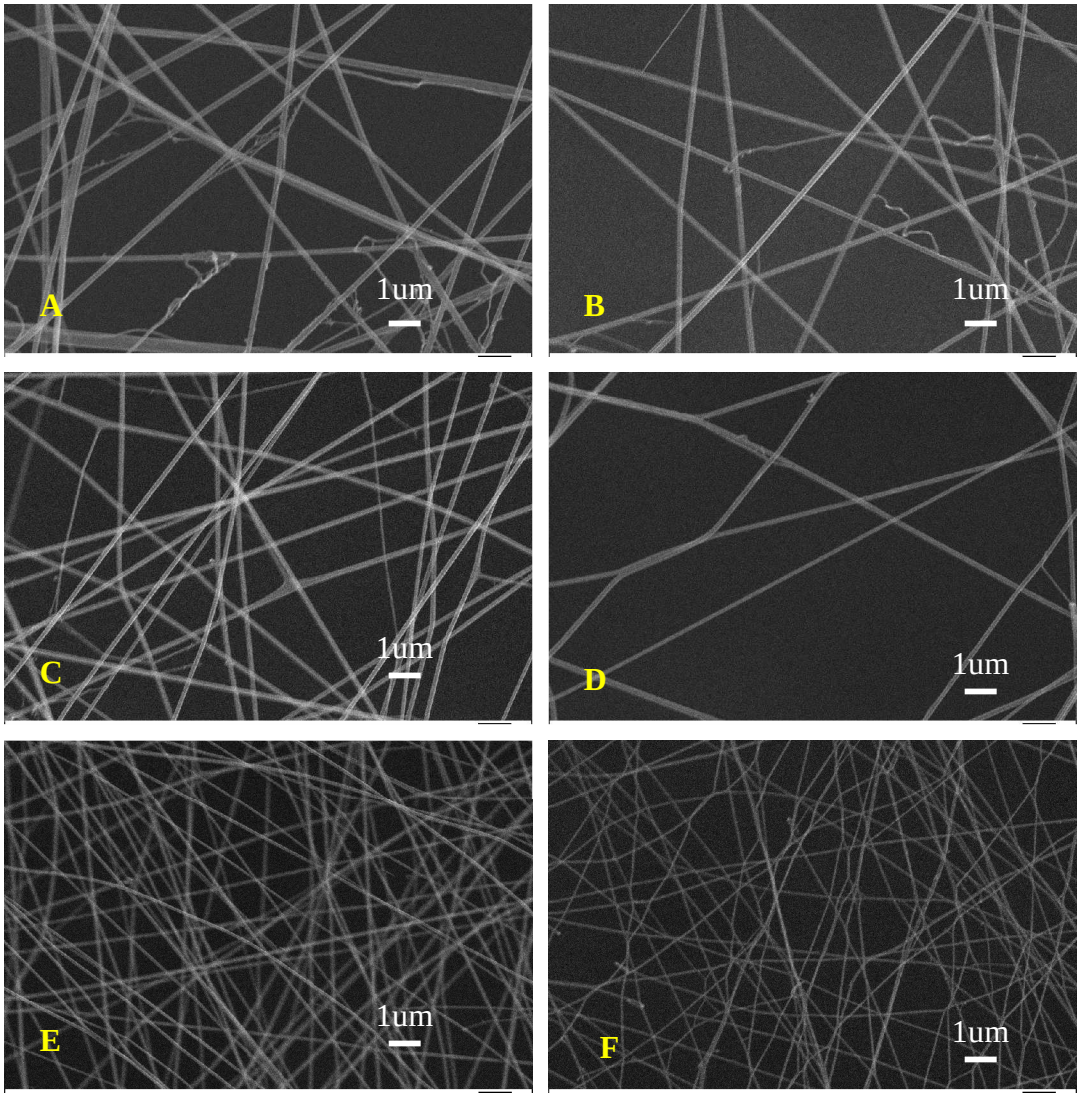

Figure 3.1 SEM images (at 20 kX) of nylon fibers made form 18% (A), 16% (B), 14% (C), 12% (D), 10% (E), and 8% (F) by weight concentration in formic acid.

The average diameters of the fibers observed were determined statistically by measuring the diameter of 20 fibers per sample using Zeiss SmartSEM^{TM} software. The diameters are listed in Table 2.1. The dependence of average fiber diameter to nylon-4,6 concentration by weight % is plotted in Figure 3.2. An exponential relationship was fitted to the data points leading to the equation

$$D = 28e^{0.1236C}$$

where D is the average diameter (in nm) of fibers and C is weight percent of nylon-4,6 in solution. At high concentrations the diameter increases quickly with the increase of nylon-4,6 concentration. Inversely, at low concentrations the fiber diameter increases slowly with the increase of the concentration.

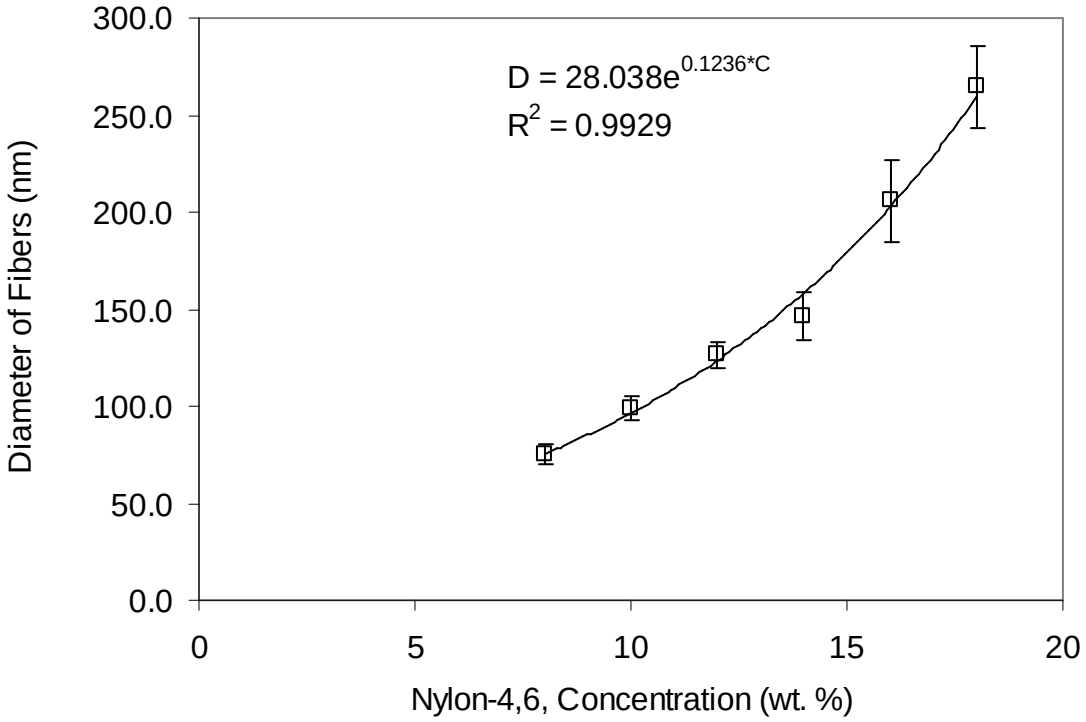

Figure 3.2 The average diameter of fibers, in nm, as a function of weight % concentration of Nylon,4-6 in solvent.

3.2.2 Fiber Beads

It was observed that some fibers of electrospun Nylon-4,6 contained defects in the form of beads, as shown in Figure 3.3 A. These beads were aligned along the fiber and varied both in size and in spacing. These beads were sometimes observed at high concentrations but were especially prevalent in smaller fibers produced at low concentrations. These beads can be explained by the relationship between the concentration, viscosity, and conductivity of the polymer solution.

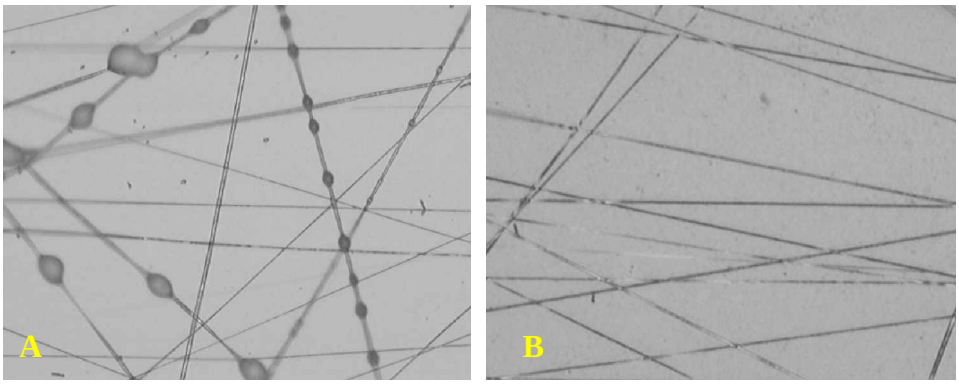

Figure 3.3 Optical images of electrospun nylon-4,6 fibers (18 wt. % in solution) showing a) "beading" in polymer solution containing no additives and b) uniform fibers in polymer solutions containing 0.4 wt. % pyridine.

Polymer solutions can be categorized into three concentration regimes, the diluted regime, the semi-diluted regime, and the concentrated regime.[2] Within the concentrated regime molecular chain entanglement is prevalent resulting in an increase of the solution viscosity. It has been shown that polymer solutions with high viscosity produce relatively thick fibers that are free of beads.[3] In the diluted regime polymer molecules have a coil-like structure, which can be approximated as separated spheres. Due to these, tight, coil-like molecular structures, molecular entanglements are not as prevalent as in other regimes. This results in a very low polymer solution viscosity. In the semi-diluted regime molecules retain a coil like structure but are crowded. This leads to a higher interaction rate between molecules and consequently an increase in entanglement and solution viscosity. It has been shown that beads form during electrospinning while the jet is still

fluid if the electrical field that acts to extend the fiber is momentarily disrupted [4]. Such a disruption can occur if ions created in air from local corona discharge neutralize the electric charge of the fiber jet. The surface tension of the jet can then create enough pressure to force the formation of a bead.

One method by which the formation of beads can be reduced is by increasing the electrical conductivity of the polymer solution so that the electrospinning jet has the ability carry more charge and thus be less susceptible to neutralization. This has been experimentally verified by Magarvey and Outhouse who found that the breakup of a water jet is reliant upon the electrical current.[5] It was shown that with increasing current of the water jet the formation of droplets is reduced.

The conductivity of solutions used in this study was increased by adding small amount of pyridine. Pyridine is a base and reacts with formic acid to produce an organic salt of a weak acid and a weak base.[6] Figure 3.4 graphs the electrical conductivity of nylon-4,6 in formic acid with and without the addition of 0.4 wt. % pyridine.

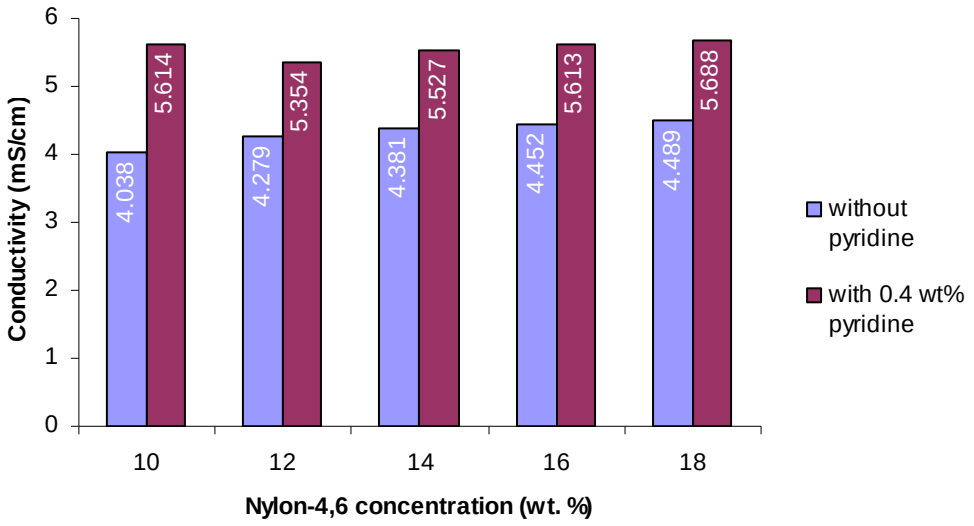

Figure 3.4 Graph comparing solutions containing various concentrations of nylon in formic acid, with and without 0.4 wt. % pyridine.

The pyridine was shown to have a significant influence on the conductivity of the various solutions of nylon-4,6 in formic acid. Without the addition of pyridine the conductivity of the solutions decreased slightly with a decrease in nylon-4,6 concentration. The addition of pyridine to the solutions raised the conductivity at all concentrations. A larger percentage change in conductivity was observed in solutions containing low concentrations of Nylon-4,6. At a 10% wt. concentration the raise in conductivity is nearly 40%. As the wt. % of nylon-4,6 is increased the conductivity is still raised but the effect is less pronounced. Solutions containing 18% nylon-4,6 by weight had a 26% increase in conductivity. The conductivity and resistance of all solutions studied are listed in Table 3.2.

nylon-4,6 Conc. (wt. %)	pyridine conc. (wt. %)	conductivity (mS cm^{-1})	resistance (Ohm*cm)
10	0	4.038	247.2
12	0	4.279	233.6
14	0	4.381	228.4
16	0	4.452	224.6
18	0	4.489	222.9
10	0.4	5.614	178.2
12	0.4	5.354	186.7
14	0.4	5.527	180.9
16	0.4	5.613	178.2
18	0.4	5.688	175.8

Table 3.2 The pyridine concentration and electrical conductivity of various solutions used.

As pyridine is added to the solution the conductivity is increased and the electrical resistance is decreased because the concentration of ions, responsible for carrying current in solution, is increased. As the concentration of pyridine in solution is increased the conductivity continues to increase. A solution of 18 wt. % nylon-4,6 was investigated with varying pyridine concentration. The results are shown in Figure 3.5. The relationship between pyridine concentration and conductivity is linear and can be expressed by

$$K = 2.93 * C_p + 4.4$$

where k is the electrical conductivity and C_p is the pyridine concentration in wt. %. It was observed that the formation of beads was decreased with the increase of pyridine

concentration. With the addition of 0.4 wt. % pyridine the formations of beads were avoided in all nylon-4,6 concentrations above 10 wt. % in solution. Studies by Huang et al. have reported that adding pyridine to a solution of Nylon-4,6 in formic acid has no influence on the viscosity and little influence on the surface tension.[6]

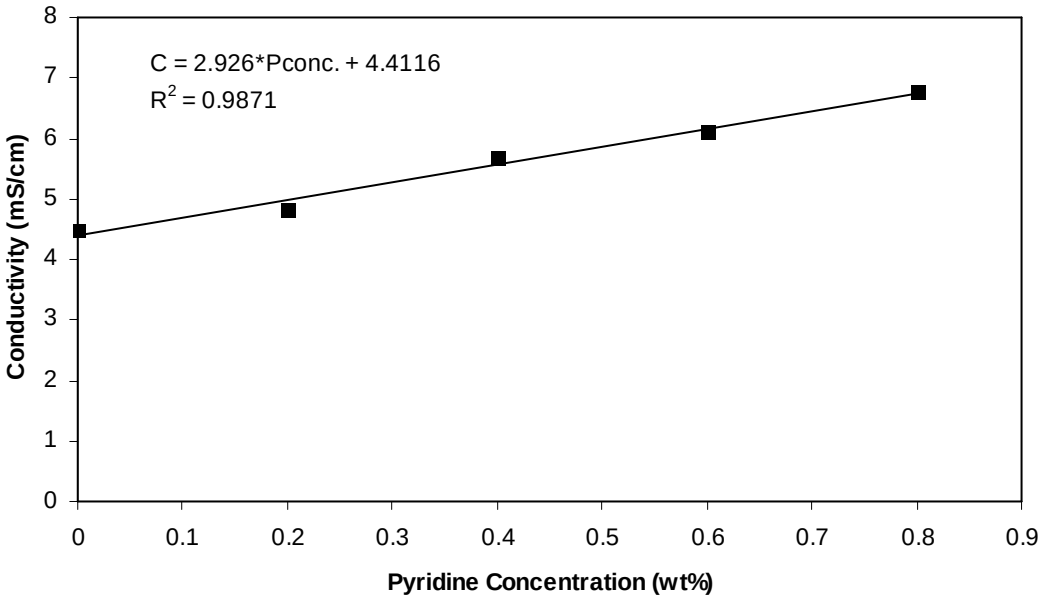

Figure 3.5 Conductivity of a 18 wt. % nylon-4,6 in formic acid solution at varying pyridine concentrations.

3.3 Mat Morphology

The mat morphology of was investigated by electrospinning nylon-4,6 onto a variety of different substrates as outlined in Chapter 2. Initial tests indicated that fiber deposition was not uniform. Some mats were observed to show signs of surface reorganization. That

is, fibers deposited close to one another would branch and fuse together. It was also discovered that electrospun fibers appeared to avoid depositing on dielectric substrates with a small surface areas. Fibers collected at a significantly higher rate on the grounded drum than on the substrate. Finally it was noted that fibers deposited onto a wide variety of substrates did not produce uniform layer even at extended deposition times. Fibers collected preferentially in certain regions of the substrate but avoided others.

3.3.1 Fiber Branching

Several samples were prepared by electrospinning nylon-4,6, at concentrations of 8, 10, 12, 14, 16 and 18 wt. %, onto a polyester substrate (P-20) for 20 minutes. The pyridine concentration was 0.4 wt. %. SEM images of the samples were analyzed and it was observed that at the lowest nylon-4,6 concentration, 8 wt. %, fibers are interlinked. Short segments of fibers are fused between the larger fibers which primarily comprise the mat, see Figure 3.6. The same mat also showed a small amount of beads along the primary fibers. The branching fibers were only observed along fibers that contained these beads. This effect was not observed at any concentration above 8 wt. %, and it should be noted that these samples also showed no signs of beading. Similar branching has been observed by Hung et al., however no explanation is provided[6].

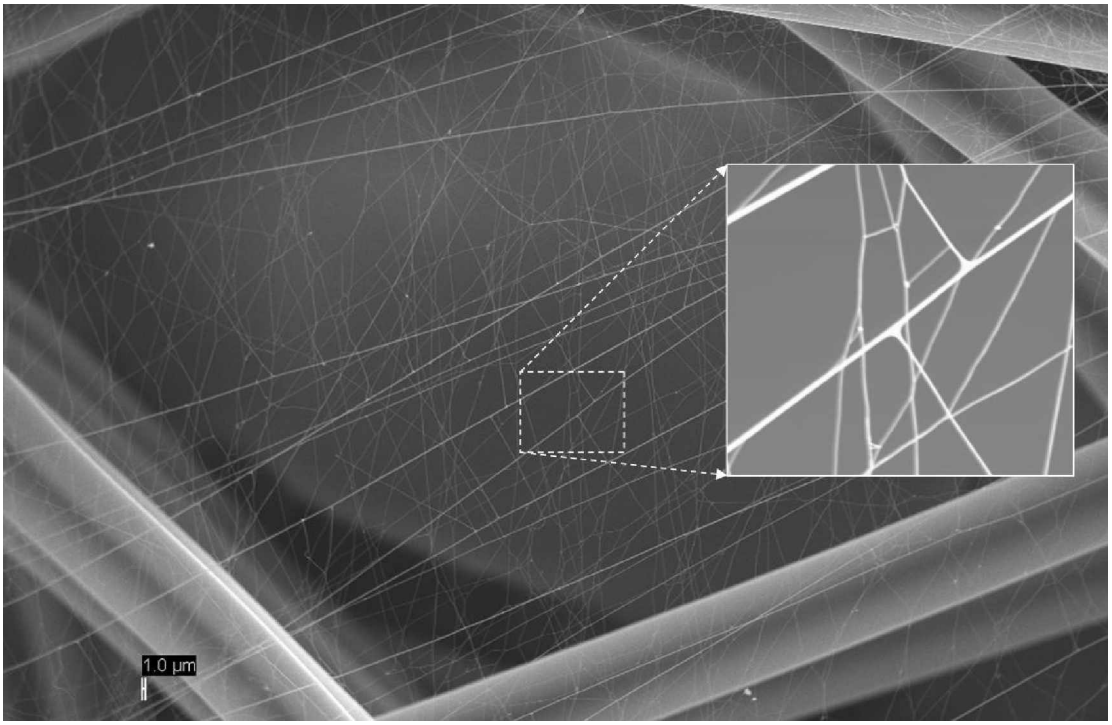

Figure 3.6 SEM images (500X and 4.5kX) showing branching of collected fibers (Solution:18 wt. % nylon-4,6, in FA; Substrate: polyester (P-20).

It was not conclusively determined what causes the branching in this work. One possibility is that splaying of the fibers occurs before deposition while the polymer jet is in the whipping regime. If the fibers are not fully solidified upon deposition fusion between fibers is possible. This explanation, however, seems unlikely as the connecting fibers are observed to clearly terminate at each end between the primary fibers and do not propagate further as would be expected if two crossed fibers fused or entangled. Another hypothesis is that the fibers contained a significant amount of charge upon deposition allowing additional polymer jets to form at the fibers surface. The SEM images suggest

that this is a possibility as the area where the connecting fiber emerges from the primary fiber has a jet like formation. It cannot be determined if this jet-like formation occurs only in locations that previously contained a bead. This effect was also not observed in previous experiments in which beads occur at higher concentrations without the addition of pyridine.

3.3.2 Surface charging

Surface charging is an effect that occurs as charge, carried from electrospun fibers, is transferred to the substrate during deposition. Although the drum onto which the substrate is attached is grounded, surface charging may still occur. This is due to the fact that charge may be deposited at a higher rate than the removal rate due to charge flow into the drum. This effect becomes especially problematic when electrospinning onto a dielectric substrate. At the onset of electrospinning, fibers will deposit onto the dielectric substrate because of their electrostatic attraction to the grounded collection plate located behind it. Each fiber that is initially collected will deposit some charge, of the same polarity as the electrospinning voltage, onto the substrate. Within a very short period of time the substrate will reach a critical saturation point at which no further deposition occurs due to electrostatic repulsion between the positively charged fibers and the positively charged substrate. The total amount of charge deposited by the electrospun fibers onto the collection drum was determined by measuring the voltage drop across a 1MOhm resistor, connected in series between the collector and ground, using digital multimeter. The results are reported in Table 3.3

Nylon Conc. (wt. %)	18	16	14	12	10	8
Fiber Current (nA)	214 ±25	202 ±18	107 ±8	98 ±9	85 ±5	67 ±4

Table 3.3 Current measured on the collection drum as a function of nylon concentration.

This effect of surface charging was observed when 18% wt. nylon-4,6 was electrospun onto a dielectric substrate. The collection drum was wrapped in a single layer of aluminum foil onto which the substrate, a circular disc of polyester (P-20) cut to a ½" diameter, was attached using two strips of copper tape. The electrospun fibers were deposited for a period of 10 minutes. As shown in Figure 3.7a electrospun fibers did not collect on the dielectric substance with any significant quantity. The mat of electrospun fibers can be seen as a white mat covering the aluminum foil. This region has a dense deposition of fibers as seen under SEM imaging in Figure 3.7b. A ring of about 1mm in width surrounds the substrate and marks the perimeter of the area in which very few fibers are collected. This is verified by the SEM image shown in Figure 3.7c.

In order to increase the deposition of electrospun fibers onto dielectric substrates disc a corona apparatus was devised. Using this method the substrate could be neutralized of excess charge. It is discussed in detail in section 2.5 of this chapter.

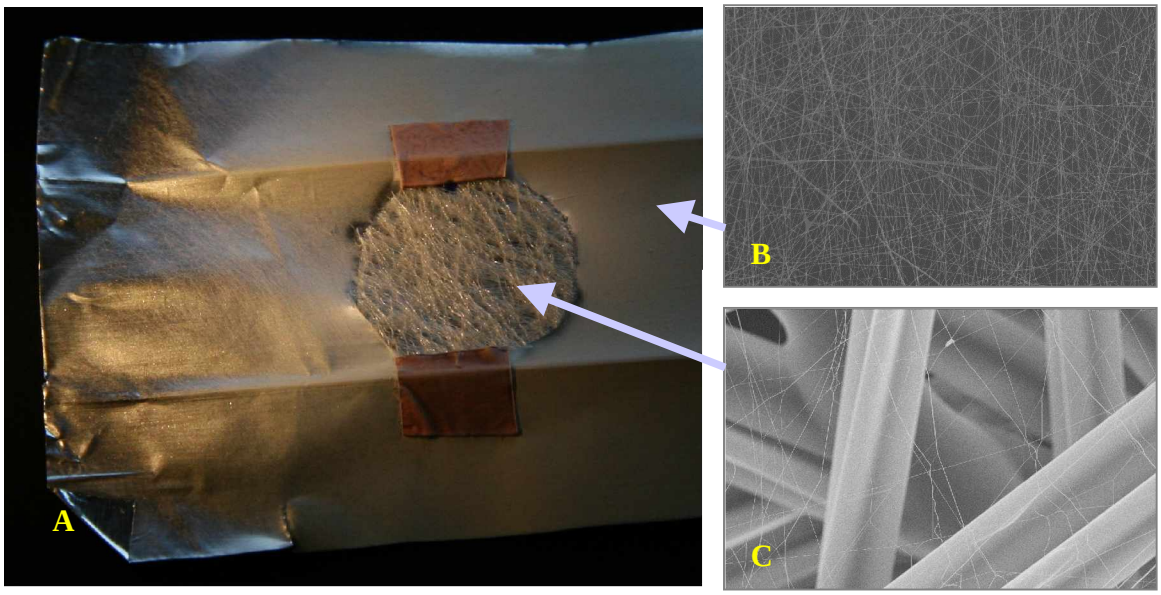

Figure 3.7 Images of 18 wt. % nylon-4,6 electrospun onto a ½" disc of polyester (P-20) attached to a sheet of aluminum foil via Cu tape. A) Optical image of aluminum and polyester substrate. B) SEM images (2kX) of the aluminum region. C) SEM image (2kX) of the polyester disc.

3.3.3 Substrate selection

Various substrates, as outlined in Chapter 2: Table 2.3, were selected and evaluated for use as the support structure for the electrospun filter mats used in this work. Figure 3.8 shows SEM images of nylon-4,6 being spun onto (A) cellulose, (B) polyester, (C) polypropylene, (D) fiberglass, (E) stainless steel, and (F) nylon. All samples were cut to ½" discs and were attached to the hexagonal collection drum using two strips of Cu tape. After electrospinning a layer of fibers was observed to have collected within a 4-5 cm

band centered at the substrate disc. Samples were removed by cutting off the two pieces of Cu tape using an uncoated razor blade. The razor was then used to cut around the perimeter of the substrate after which the sample could be lifted from the collector using tweezers.

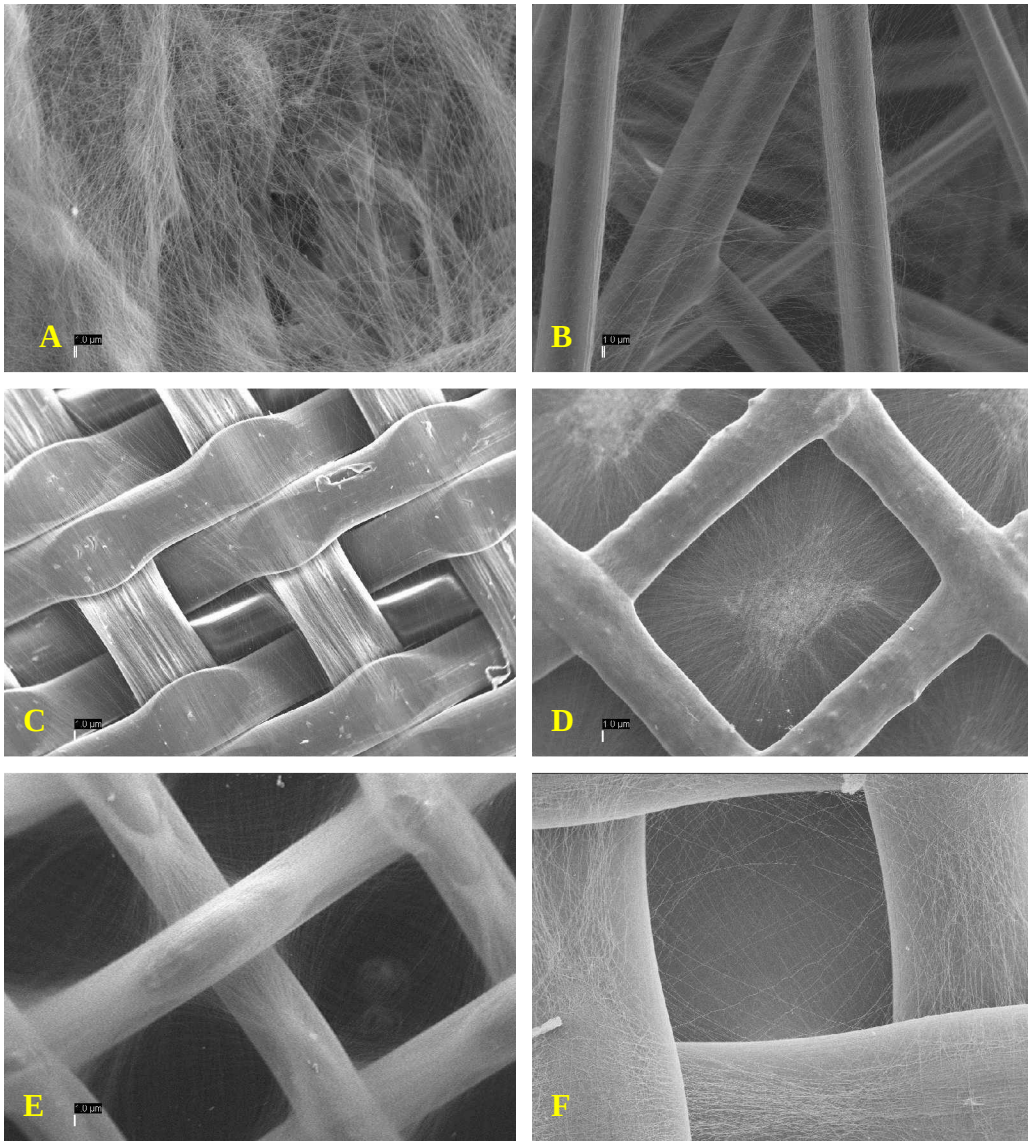

Figure 3.8 SEM images of various substrates with electrospun nylon-4,6 fiber deposition; A) cellulose, B) polyester, C) polypropylene, D) fiberglass, E) stainless steel, and F) nylon.

Electrospun layers of nylon fibers were not uniform in any of the substrates evaluated. In the case of the two non-woven substrates, cellulose and polyester, fewer fibers were collected in areas of the substrate material that were less dense (i.e. areas that contained fewer polyester or cellulose fibers). Areas in which the substrate was thicker had a much denser layer of electrospun fibers. This resulted in an uneven distribution and areas with little or no electrospun fibers were found. The polypropylene substrate has a double weave pattern that is very densely spaced. It was found that the fibers collected were very aligned but, as in the previous cases, distributed unevenly. Rows of fibers are seen between areas of the substrate that are raised, while other areas have little or fiber deposition. The fiberglass has an evenly spaced square weave pattern but is produced using heating and pressure treatments that fusses overlapping threads. This results in a woven layer that is much more consistent in local thickness than traditional weaving. In this sample fibers were found to align themselves from the edge to the center of individual opening. The central region consisted of an area of random fiber orientations. The final two substrates evaluated, nylon and stainless steel, have a standard square weave square. Here fibers are observed to “hug” the corners of the individual weave openings. The fibers collected in this region are also observed to be aligned. The central regions of the opening had very little fiber deposition.

It is hypothesized that this uneven distribution on all of the substrates tested can be attributed to the effects of charge dissipation of deposited fibers by the substrate. The first layer of fibers is thought to deposit uniformly across the surface of the substrate. However, fibers that are collected on the physical threads that make up the substrate are believed to loose charge while those suspended in open regions retain charge. This is possible, even in the polymer substrates as they do not act as perfect insulators. A small amount of charge can still seep off into the grounded collection drum. Suspended fibers are thought to retain charge for a longer period of time. This creates an electrostatic imbalance between the open and solid areas of the substrate. Positively charged electrospun fibers that reach the substrate after the initial layer of deposition will be slightly repelled by the positively charged suspended fibers and collect preferentially on the substrate threads. This explains why many fibers are seen in solid regions while relatively few fibers are observed in open areas or less dense regions.

3.4 Corona Assisted Deposition

3.4.1 Introduction

A corona apparatus, as described in Chapter 2, was used to eliminate the surface charging effects reported in this chapter. A corona is created when a high voltage is placed on a sharp point. Charge concentrated in this location causing ions of equal polarity to the corona voltage to be expelled. In the experimental apparatus used in this work a corona, consisting of a hypodermic needle connected to a HV negative power supply, is placed

opposite the collector with respect to the electrospinning needle. As high voltage is applied negatively charged ions begin to bathe the collector and filter substrate. The substrate is attached to the electrospinning collector consisting of a rotating hexagonal drum. As the drum is rotated positive charge from the electrospun fibers is collected on the substrate. This charge is, however, neutralized by corona ions as the collector completes its rotation. Figure 3.9a, shows the initial configuration of the corona apparatus. While the ions did neutralize the substrate, some ions migrated towards the opposite side of the collector. As these negatively charged ions reached the positively charge electrospun fibers, charge neutralization occurred. The electrospun fibers, now neutralized, lost momentum as the electrostatic attraction to the grounded collector was lost. As shown in Figure 3.9b the corona apparatus was modified to include a shield, consisting of a grounded electroformed wire mesh. This mesh prevented ions from flowing in all directions except a single face of the collection drum. Other ions are neutralized by the grounded shield and prevented from migrating past the collector.

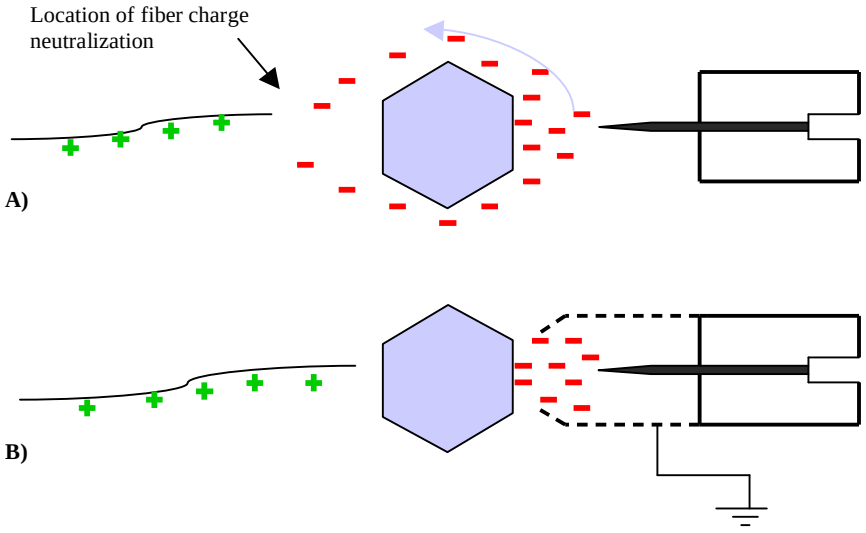

Figure 3.9 Cross-sectional schematic diagrams showing corona ion flow towards the electrospinning apparatus with A) no corona shielding and B) grounded corona shielding.

3.4.2 Surface Charge Neutralization

It was experimentally observed that the substrate was electrically neutralized by the corona. As previously described a ½" disc of polyester substrate was attached to a sheet of aluminum foil wrapped around the collector. Electrospun fibers are deposited on the substrate for 10 minutes with and without corona. A +7.5kV and -4.5kV is applied respectively to the electrospinning needle and corona. As shown in Figure 3.10 the sample without corona had very little deposition on the polyester disc but fibers are collected on the aluminum foil indicating that surface charging occurs. The samples for which a corona was used showed fiber deposition on the aluminum substrate as well as the polyester disc. At high SEM magnification it was also observed that the electrospun

mat collected on the substrate with corona had a very uniform fiber mat, indicating that the effects of image charging by the fibers on the substrate were eliminated.

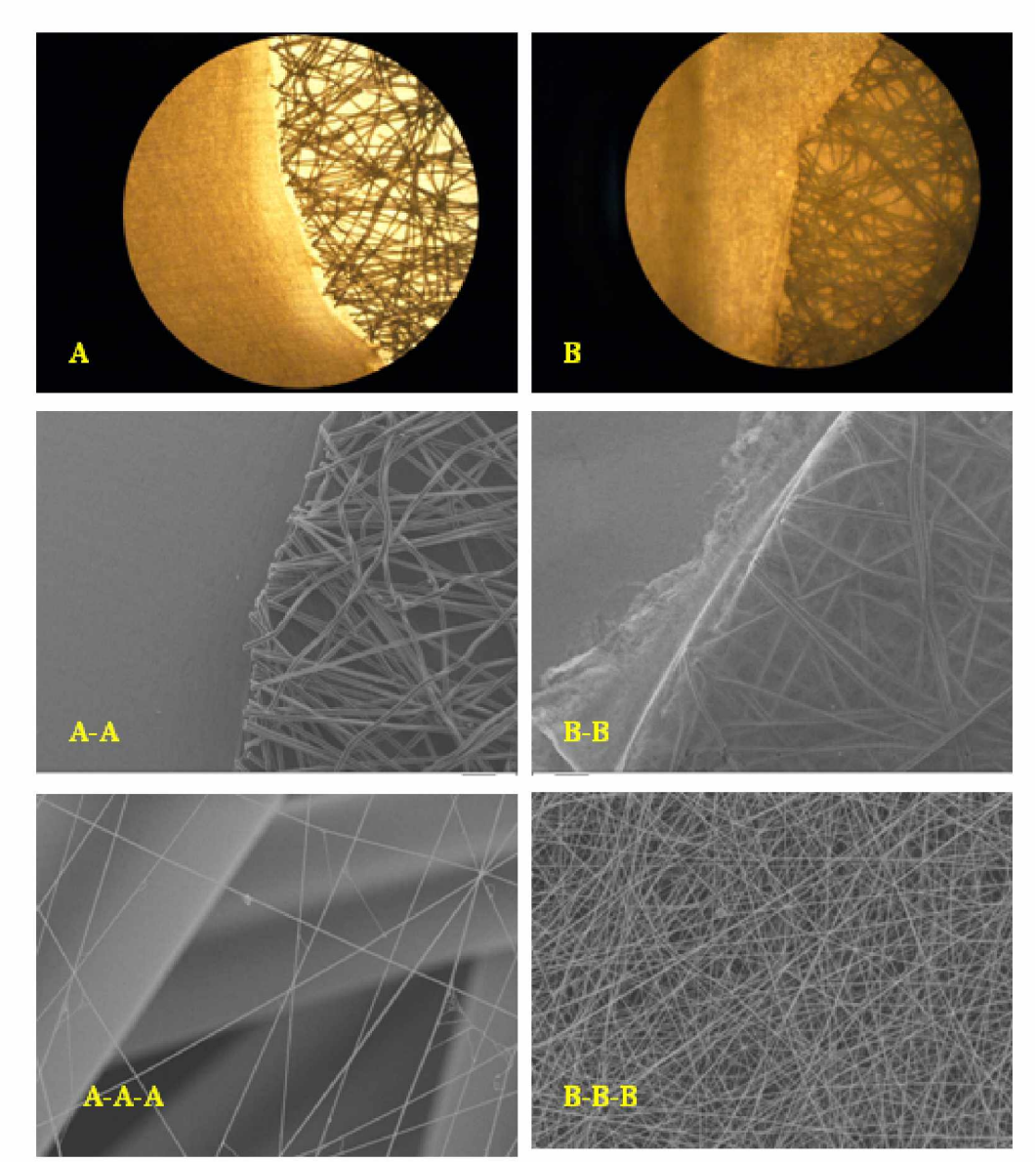

Figure 3.10 Images of nylon-4,6 fibers electrospun onto a ½" disc polyester substrate with and without the use of corona . Optical microscopy images at 20X are shown for two samples; (A) without corona and (B) with corona. SEM images at 80X magnification

of the same samples are shown in figures (A-A) and (B-B). SEM images at 2kX of the polyester surfaces of both samples are shown in (A-A-A) and (B-B-B).

3.4.3 Corona Distance and Voltage Dependence

The current that is collected on a substrate due to corona was investigated. Two ½" discs, one Cu foil and the other a 1 mm thick Teflon^{TM}, were glued together. The Teflon^{TM-} side was attached using double sided Scotch tape to one face of the collection drum so that it was position directly across from the corona needle. A wire was soldered to the disc in order to measure collected current using a digital multimode. Figure 3.11 shows a graph of current collected on the disc as a function of distance between the corona needle and collector at various corona voltages. It was observed that collected current increased exponentially with decreasing distance. Currents of between 5-90 μA were observed at distances ranging from 7- 22 mm. This is one order of magnitude larger than the fiber currents measure previously. As the voltage to the corona is decreased the collected current also decreases as expected since less corona ions are produced.

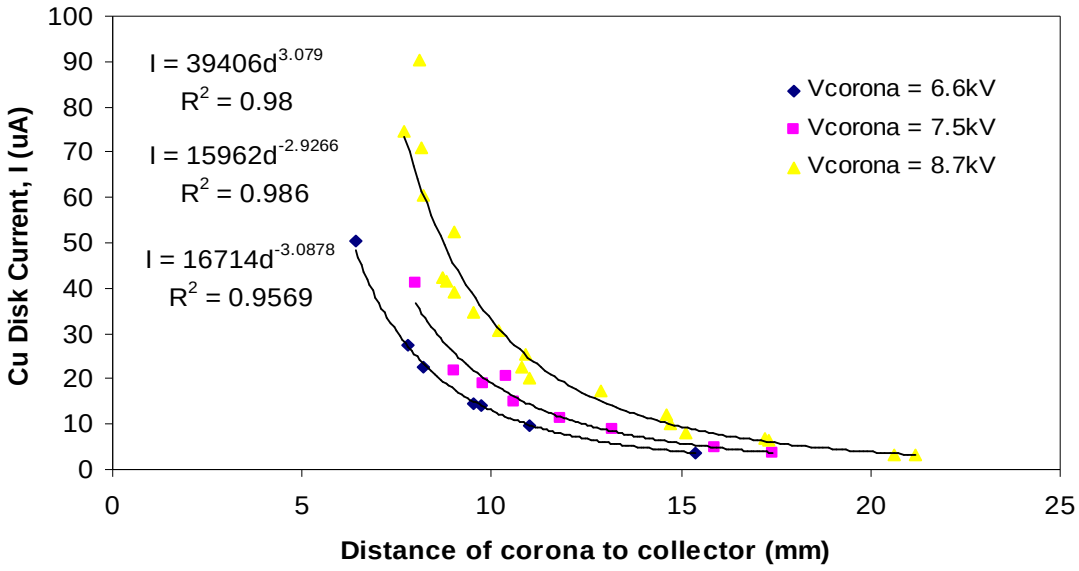

Figure 3.11 Current collected on a ½"Cu disc attached the collector as a function of corona to collector distance and voltage.

3.4.4 Coronas Effect on Fiber Size

It was observed that the use of corona has an effect on the average diameter of the electrospun fibers. A solution of 16 wt.% nylon-4,6 was electrospun onto a nylon substrate (N-305) cut to a ½" diameter disc for a period of 10 minutes at various corona voltages. As shown in Figure 3.10 the corona voltage was varied from 2kV to 4.5kV. The average fiber diameters listed in Table 3.4 and graphed in Figure 3.13. At the lowest corona voltage studied, 2kV, the average fiber diameter is close to the expected value of around 200 nm determined previously. As the corona voltage is increased it is observed that the average fiber diameter decreases. The largest corona voltage, 4.5kV, fibers have an average diameter of 133 nm. It should be noted that at 2.3kV an increase in fiber diameter was observed. This may be due to the fact that the image was taken near the

edge of the sample were the electrospun fibers were cut and fibers deform. The explanation for this overall decrease in fiber diameter may be linked to the negative charge placed on the substrate by the corona. This charge may increase the electrostatic filed between the fiber and collector resulting in increased elongation.

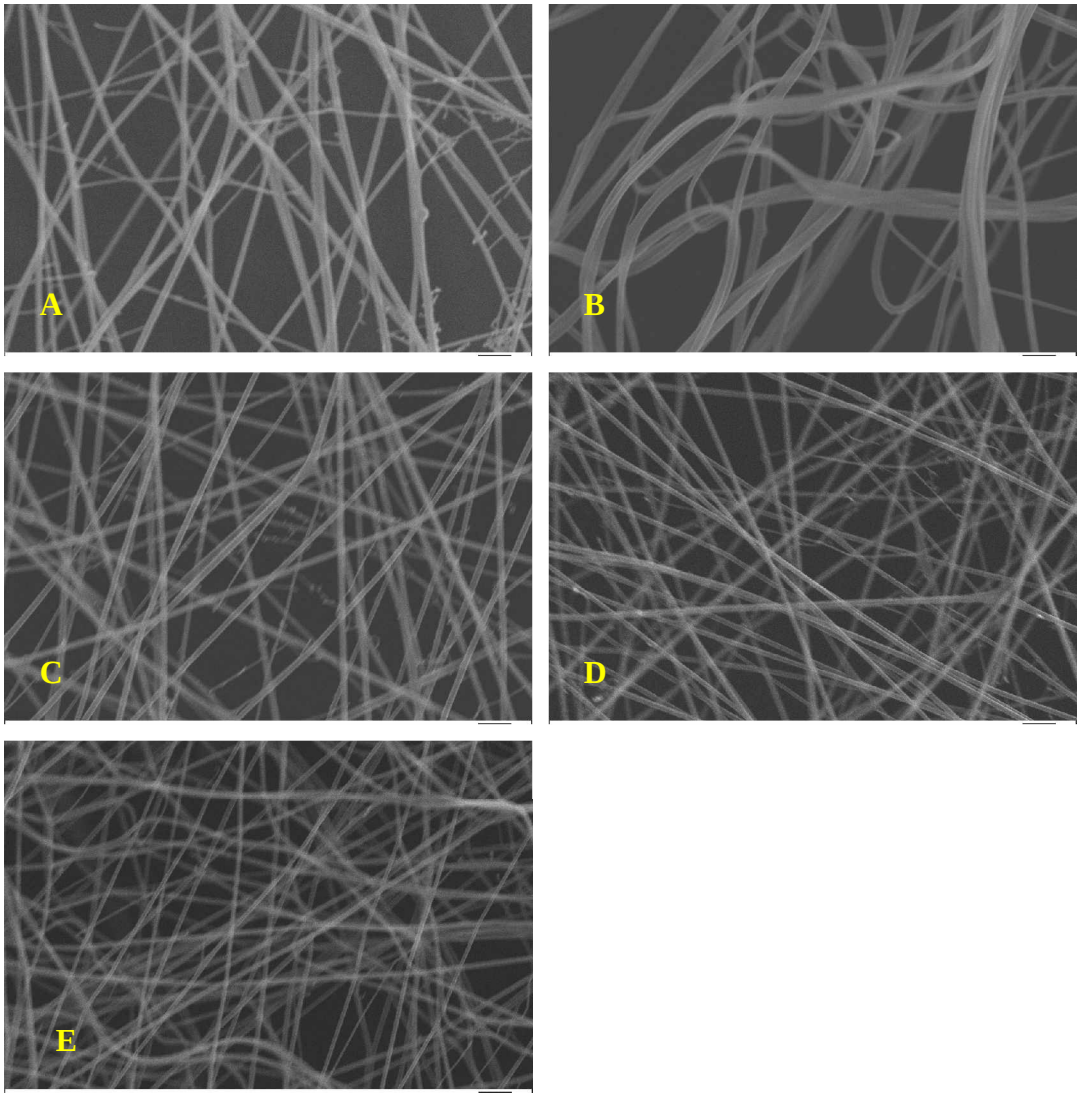

Figure 3.12 16% nylon electrospun onto the N-305 substrate at (A) 2kV, (B) 2.3kV, (C) 2.6kV, (D) 3kV, and (E) 4.5kV corona intensity

Corona Voltage	2	2.3	2.6	3	4.5
Diameter of fibers (nm)	200 ± 24	231 ± 25	189 ± 21	162 ± 15	133 ± 13

Table 3.4 Average fiber diameters of electrospun Nylon-4,6 (16 wt.%) at various corona voltages.

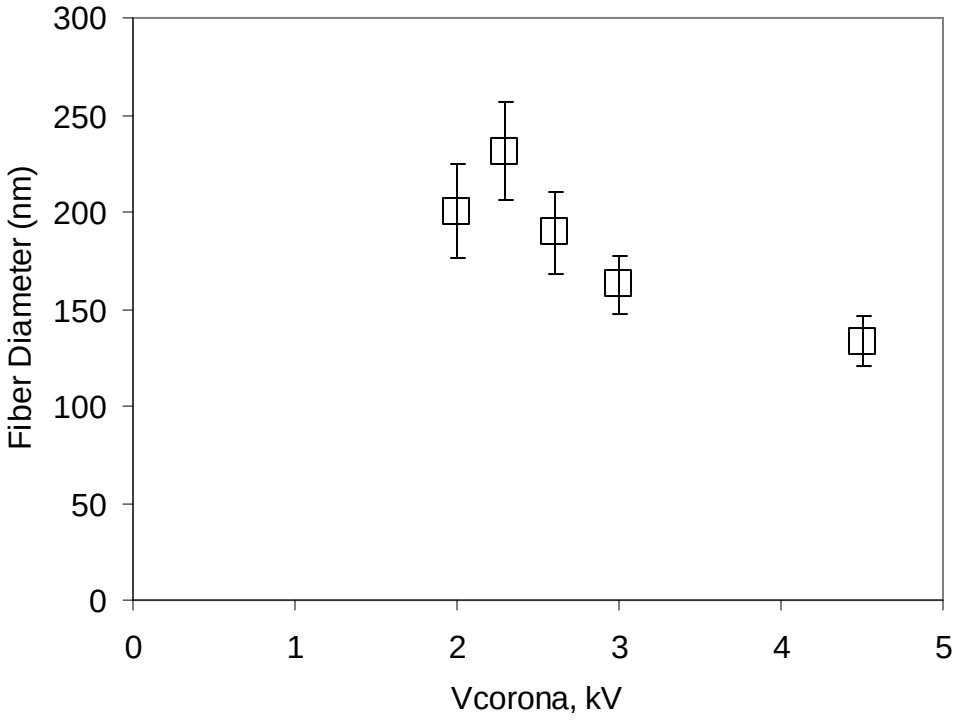

Figure 3.13 Graph of fiber diameters of electrospun Nylon-4,6 (16 wt.%) as a function of corona voltage.

3.4.5 Conclusions

Fibers were created at a variety of diameters by controlling the nylon-4,6 concentration in solution. Beading was prevented by adding a small amount of pyridine, typically 0.4 wt. %, to the electrospinning solution to increase conductivity. Samples were shown to have non-uniform fiber deposition due to surface charging effects. These effects were eliminated through the use of a corona which neutralized the substrate. This charge neutralization effect was observed in all samples used analyzed this work. Cellulose, polypropylene, polyester, fiberglass, stainless steel, and nylon were coated uniformly with fibers and did not show signs of substrate avoidance by the electrospun fibers.

Chapter 4 will focus on the filtration performance of nylon-4,6 fiber mats electrospun onto selected substrates with a variety of fiber diameters. Filtration efficiency, pressure drop and Figure of Merit are reported.

Bibliography

1) Bergshoef M M and Vancso G J 1999 *Adv. Mater*. 11, 1362.

2) Doi M. "Introduction to Polymer Physics". Oxford Press, Clarendown. 1996.

3) Fong H and Reneker D H. 1999 *Polymer*. 40, 4585.

4) Fong H, Chun I and Reneker D H. 1999. Elastomeric nanofibers of styrene-butadiene-styrene triblock copolymer. J. Polymer Sci. B. 37, 3488-93.

5) Magarvey R H and Outhouse L E. 1962 *Journal of Fluid Mechanics.* 13, 151-7.

6) Huang C. et al. "Electrospun polymer nanofibers with small diameters", Nanotechnology. 17. 2006, 1558-1563.

CHAPTER 4

FILTER PERFORMANCE TESTING

4.1 Introduction

The filtration performance of various electrospun nylon-4,6 mats were evaluated. Filters were evaluated for particle capture efficiency, the pressure drop across the filter and the calculated Figure of Merit (FOM). Electrospun filters produced in this study were also compared against commercially available high performance filters.

4.2 Sample Selection

The samples selected for use in this study consist of electrospun nylon-4,6 fibers collected on a ½" disc of nylon mesh (N-305). As shown in Table 4.1 the electrospun fibers were produced at three average fiber diameters of, 265, 147, and 99 nm, by varying the weight concentration of nylon-4,6 in formic acid from 18 and 10 % respectively. Each polymer solution contained 0.4 wt. % pyridine to prevent beading of the electrospun fibers. The electrospinning voltage and corona voltage were 7.5kV and 4.5kV respectively. All other electrospinning parameters were as outlined in chapter 2. Three samples were produced for each of the three polymer concentrations by depositing fibers for a period of 4, 8 and 12 minutes.

Filter ID	nylon-4,6 conc. (%)	Deposition time, t_d (min)	Fiber diameter d_f	Solidity, α	0.3 µm Effciency, %	Pressure drop, Δp	0.3 µm FoM
ES10-4	10	4	99	0.065	89.73	200.9	0.01133
ES10-8	"	8	"	"	98.14	407.4	0.00978
ES10-12	"	12	"	"	99.07	669.8	0.00698
ES14-4	14	4	147	0.062	77.04	167.0	0.00881
ES14-8	"	8	"		98.25	560.2	0.00943
ES14-12	"	12	147		98.44	785.5	0.00456
ES18-4	18	4	265	0.04	77.16	210.0	0.00703
ES18-8	"	8	"	"	97.77	403.3	0.00943
ES18-12	"	12	"	"	97.83	840.3	0.00456

Table 4.1 Properties of the various filters produced by electrospinning Nylon-4,6 at various concentrations onto Nylon (N-310) substrates.

The material chosen for use as the substrate, the electrospun fiber support structure, was a square weave nylon-4,6 mesh N-305. This substrate was chosen over other materials primarily because it resulted in a very strong bond between the electrospun fibers and the substrate. Fibers that are collected on the substrate during the electrospinning process may contain formic acid that has not evaporated during the elongation and whipping stages. The formic acid will dissolve the nylon substrate in the same manner as the nylon used in the electrospinning solution. “Wet” fibers will therefore adhere well to the nylon substrate or any other material soluble in formic acid. Electrospun fiber mats spun onto the other support structures generally showed signs of delaminating either upon removal

from the collection drum or after a few days of storage. This effect was not seen in any of the nylon substrates evaluated.

In addition to the electrospun nylon-4,6 filter produced, three commercial filter media were evaluated; a glass fiber filter, a polyvinyl chloride (PVC) membrane filter and a polytetrafluoroethylene (PTFE) membrane filter. The specifications for these filters are given in Table 4.2. All commercial filters used are manufactured by Pall Corporation. The glass filter (part # 61630) is produced using borosilicate glass without binder. The suggested use for this filter given the manufacturer is for air monitoring and gravimetric analysis. The PVC filter (part # GLA-5000) is a membrane based filter for monitoring airborne metals, silica and dust. The PTFE (part # R2PL047) filter is a Teflo^{TM} membrane based filter with a polymethylpentene (PMP) support ring used in the filtration of gases and organic solvents. All commercial filters evaluated meet NIOSH and OSHA specifications for air filtration. The claimed efficiency for removing 0.3 µm particles for the glass, PVC, and PTFE filters are 99.98%, 99.79% and 99.94% respectively at 32 L/min/100 cm^2 following ASTM D 2986-95A.

Filter ID	Pall part #	Type	Pore Size[1], µm	Air Flow Rate[1], L/min/cm^2	0.3 µm Efficiency, %	Pressure drop, Δp	FoM
Pall_Glass	61630	Glass Fiber	1	60	95.11	1381.9	0.00359
Pall_PVC	GLA-5000	PVC Membrane	5	53	96.96	1425.5	0.00245
Pall_PTFE	R2PL047	PTFE Membrane	n/a	17	99.30	1027.1	0.00483

Table 4.2 Properties of the various commercial filter media evaluated in this study. [1]From manufacturer's specifications sheet.

4.3 Filtration Testing

4.3.1 Conditions

Filters evaluated in this study were placed in the Filter Test Rig (FTR) described in Chapter 2. Two rubber O-rings are placed on either side of the filter. This produces a tight seal between the upper and lower piece of the FTR and the filter. The particle count bins of the Optical Particle Counter (OPC) were set to 0.3, 0.4, 0.5, 0.7, 1.0 and 2.0 µm and all measurements were taken at a flow rate of 2.8 Lpm. The sampling time for each run was set at 2 minutes with a 1 minute delay between consecutive measurements. A background particle count, obtained by running the OPC for 2 minutes without a sample present, was conducted at 5 minute intervals during testing. A zero check of the OPC was conducted before each experiment. Pressure drop was determined by taking the difference of the output values of the procure transducers placed upstream and downstream of the sample as described in Chapter 2.

A background particle count study was conducted to determine the change in particle concentration present in the lab, containing the testing apparatus, over time. The OPC was programmed to take a background sample every 15 minutes. The sample duration was 2 minutes. The OPC particle count bins were set to the same size ranges as used for filter testing. Figure 4.1 shows the graph of the data obtained. Small particles, those ≤0.5 µm, were found to have a steady concentration within the room throughout the testing period and the deviation between individual tests was small. Larger particles, >0.5 were found to have a slightly higher deviation in particle counts between individual test. This was expected as larger particles have a faster settling velocity than smaller particles. According to Friedlander the settling velocity for a 0.5 µm and 2.0 µm particle is $1.0x10^{-3}$ cm/sec and $1.31x10^{-2}$ cm/sec respectively.[1] Any movement in the room, such as someone walking past the OPC or the HVAC system turning on, would have greater impact on the concentration of larger particles than small particles. This is because larger particles which have had time to settle will be redistributed while smaller consistently remain suspended due to air circulation. The experiment showed that the background particle concentration during tests of electrospun and commercial filters did not change significantly over the 2 minute sampling time.

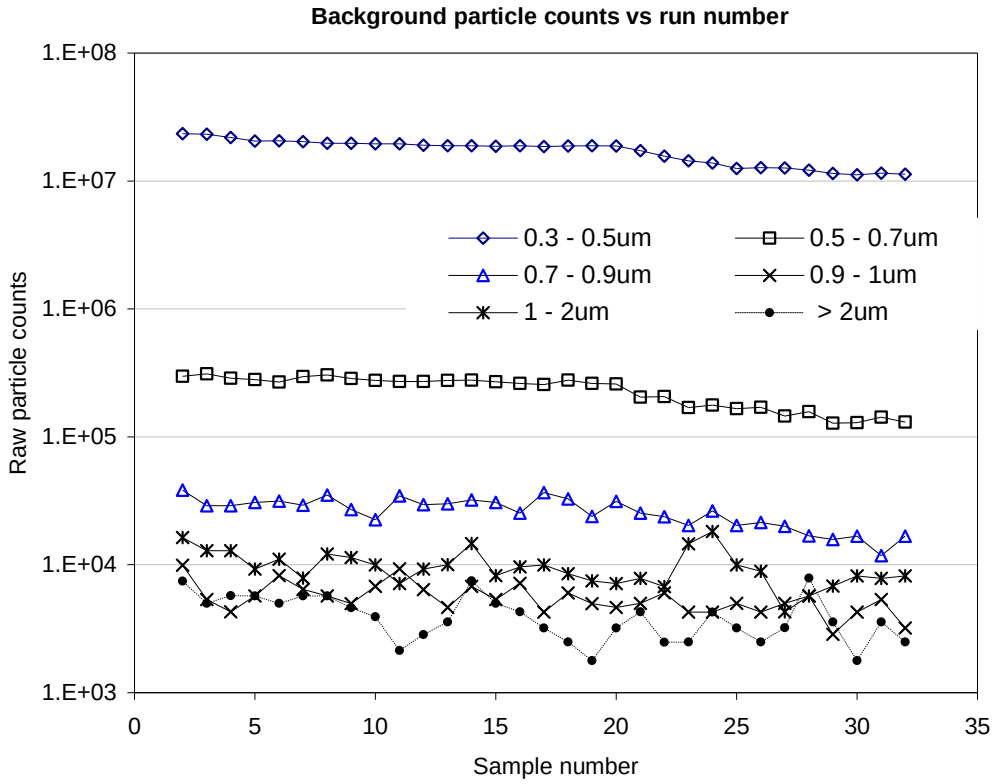

Figure 4.1 Background particle counts at 2 minutes each taken over a 6.5 hour period with a 15 minute delay between each sample.

4.3.2 Filtration Efficiency

The filtration efficiency of the electrospun filter produced in our laboratory as well as the commercial filters obtained is reported in Figure 4.2. The filtration efficiency is the percentage difference of the upstream and downstream particle concentration as described in Chapter 2. The particle size evaluated in this study is 0.3 µm. This size was chosen because it is the considered the most penetrating particle size (MPPS) and therefore the most difficult to capture. The efficiency for each of the electrospun fiber filters increased exponentially with increased deposition time as expected. It was found

that the total filtration efficiency increases exponentially as a function of deposition time. The Pall_Glass, Pall_PVC, and Pall_PTFE filters have a filtration efficiency of 95.11%, 96.96% and 99.30% respectively. The filtration efficiency of all electrospun filters with a deposition time ≥8 minutes was found to be higher than the Glass and PVC filters. The filter with the highest filtration overall was found to be the commercial Pall_PVC filter. The highest efficiency for each of the electrospun samples was at the longest deposition time, 12 minutes. ES10-12, ES14-12, and ES18-12 have a filtration efficiency of 99.07%, 98.44%, and 97.83% respectively. It is important to note that the capture efficiency increases as the fiber diameter of the electrospun filters is reduced. This is in agreement with the expectations based on an increased efficiency due to the relaxation in the no-slip condition at the surface with decreasing fiber diameter, as described in Chapter 1. As air flow around the fiber reaches a slip-flow condition an increase in efficiency can be expected because small particles, following air streams, are brought closer to the fiber surface enhancing the possibility of capture by interception.

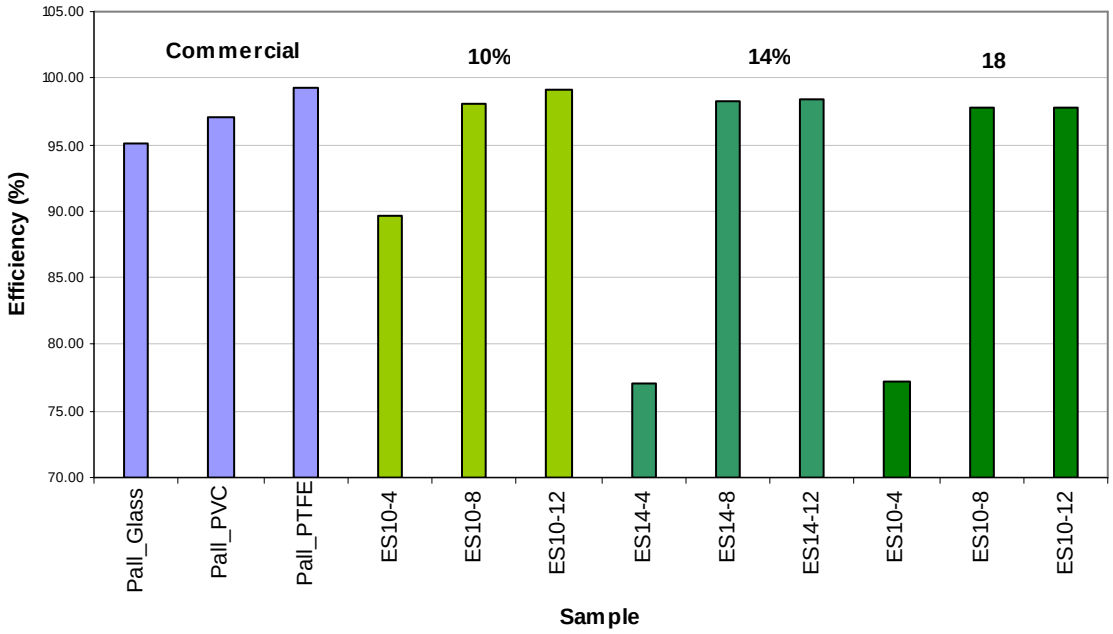

Figure 4.2 The filtration efficiency in % of particles captured at 0.3 μm electrospun filters at varying nylon-4,6 wt. % conc. and deposition times and commercial filters.

4.3.3 Pressure Drop

The pressure drop across each of the electrospun filters and the commercial filters are reported in Figure 4.3. It is observed that the pressure drop across each of the electrospun fiber filters increases linearly with deposition time. Similarly the pressure drop increases as the fiber diameter increases. This again can be attributed to the slip flow of gas around small fibers. With increasing slip-flow the pressure drop is expected to decrease due to a decrease in air drag at the fiber. When compared to the commercial filters it is observed that the electrospun fiber filters have a pressure drop that is significantly lower. This is true of all the electrospun filters evaluated.

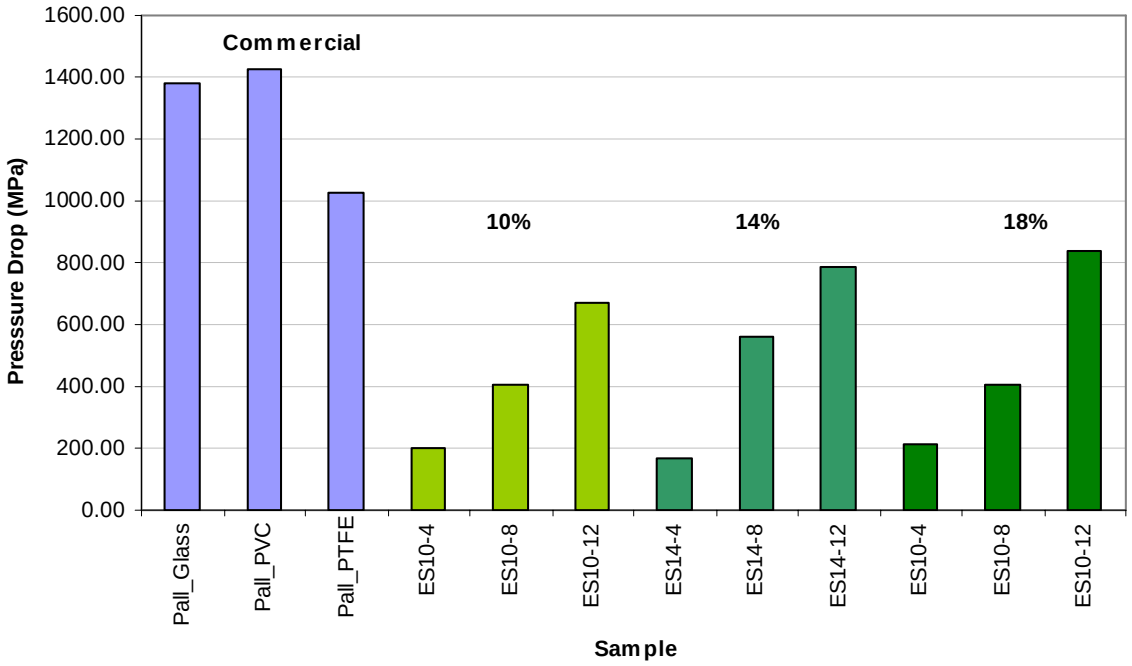

Figure 4.3 The pressure drop, in MPa, across electrospun filters at varying nylon-4,6 wt. % conc. and deposition times.

4.3.4 Figure of Merit (FOM)

The Figure of Merit (FOM) represents the ratio between efficiency and pressure drop. Generally it is desirable to have a filter with high efficiency and low pressure drop, thus larger FOM values indicate better filters. The FOM of the nine electrospun filters and the 3 commercial filters is reported in Figure 4.4. The particle size varies from 0.3 to 0.7 μm. It is noted that the filters with the highest FOM across all particle sizes measured are ES-10-12 and ES-14-12, at fiber diameters of 99 nm and 147 nm respectively. The commercial filters have a lower FOM compared to the electrospun filters with the exception Pall_PTFE. This was expected as the filtration efficiency was comparable to

the commercial filters while the pressure drop was found to be significantly lower. It is shown that for electrospun filters, smaller fiber diameters at the same deposition time result in a higher FOM. Filtration efficiency was The FOM for electrospun fiber based filters was found to be in close agreement with other experimental work investigating the figure of merit for electrospun fiber mats.[2,3,4]

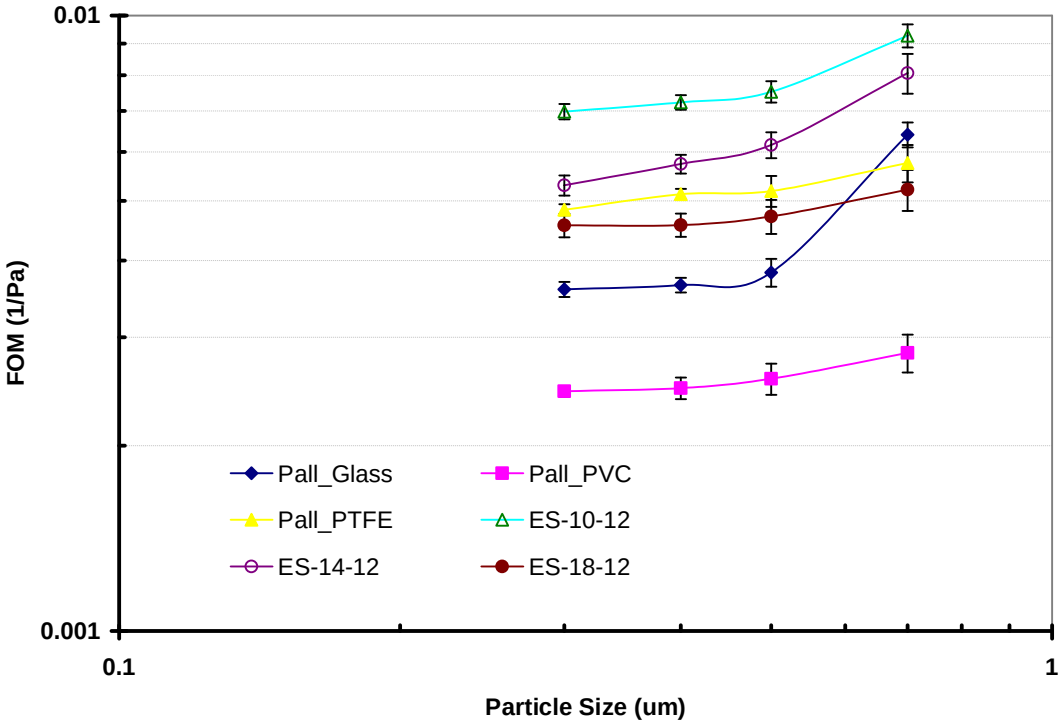

Figure 4.4 The Figure of Merit of various electrospun fiber and commercial filters for particle sizes ranging from 0.3 to 0.7 µm.

4.4 Conclusions

It was found that the electrospun fiber based filters produced in this study have an increased FOM over high-grade commercial filters. It is shown that the filtration efficiency increases exponentially with increased deposition time. It is also shown that

the electrospun fiber filters at deposition times < 8 minutes match or exceed the efficiency reported for commercial filters. The pressure drop for the various electrospun filters was found to increase linearly with increased deposition time. It is reported that the electrospun fiber filters have a significantly lower pressure drop even at the longest deposition time studied. It is believed that the increased performance in the filter efficiency, pressure drop and FOM can be attributed to the air slip-flow condition found in filters comprised of fibers having very small diameters.

Bibliography

1) Friedlander, S. K.. Smoke, Dust and Haze. 1st. New York: Wiley-Interscience, 1977. Print.

2) Ahn, Y.C. et al. “Development of high efficiency nanofilters made of nanofibers” *Current Applied Physics*. 6 (2006) 1039-1035.

3) Wang J. et al. “Investigation of the figure of merit for filters with a single nanofiber layer on a substrate”. Aerosol Science. 39 (2008) 323-334.

4) Ahn Y.C. et al. “Development of high efficiency nanofilters made of nanofibers.” Current Applied Physics 6 (2006) 1030-1035.